Pre-normative REsearch for Safe use of Liquid Hydrogen (PRESLHY)

Project Deliverable

Novel guidelines for safe design and operation of LH_2 systems and infrastructure

Deliverable Number:	D6.2
Work Package:	WP6
Version:	3.0
Author(s), Institution(s):	L. Bernard, AL, D. Houssin, AL, S. Jallais, AL, T. Jordan, KIT, D. Cirrone, UU
Submission Date:	30 April 2021
Due Date:	30 April 2021
Report Classification:	Public

FUEL CELLS AND HYDROGEN
JOINT UNDERTAKING

This project has received funding from the Fuel Cells and Hydrogen 2 Joint Undertaking under the European Union's Horizon 2020 research and innovation programme under grant agreement No 779613.

History		
Nr.	Date	Changes/Author
1.0 - Draft	27.4.2021	Original version by Laurence Bernard
1.1	29.4.2021	Additional comments from Donatella Cirrone, Thomas Jordan
2.0	30.4.2021	Version 2.0 by L. Bernard
2.1	19.5.2021	Additional comments from Pratap Sathiah, Mike Johnson
3.0	31.5.2021	Version 3.0 by L. Bernard

Approvals			
Version	Name	Organisation	Date
1.1 - Draft	Donatella Cirrone	UU	30.4.2021

Acknowledgements

This project has received funding from the Fuel Cells and Hydrogen 2 Joint Undertaking under the European Union's Horizon 2020 research and innovation programme under grant agreement No 779613.

Disclaimer

The data management in the PRESLHY project follows the principle of data management, which shall make data Findable, Accessible, Interoperable and Re-usable (FAIR). The plan for FAIR data management as described in this document is based on the corresponding template for open research data management plan (DMP) of the European Research Council (ERC).

Despite the care that was taken while preparing this document the following disclaimer applies: The information in this document is provided as is and no guarantee or warranty is given that the information is fit for any particular purpose. The user thereof employs the information at his/her sole risk and liability.

The document reflects only the authors' views. The FCH JU and the European Union are not liable for any use that may be made of the information contained therein.

Key words

Guidelines, liquid hydrogen safety.

Publishable Short Summary

This document provides easy to use guidelines to engineers for the safe design and operation of liquid hydrogen (LH_2) infrastructure.

The PRESLHY project is a pre-normative project investigating knowledge gaps related to the use of liquid hydrogen in new applications. Three main topics were addressed:

- Cryogenic hydrogen release and dispersion,
- Ignition of cryogenic hydrogen mixtures,
- Combustion of cryogenic hydrogen.

These topics were studied through:

- A review of the existing state of the art and a ranking of the identified phenomena,
- A large experimental program covering the prioritized phenomena,
- The evaluation and validation of analytical and numerical approaches to assess these phenomena.

General rules, best practices and new means to assess the consequences of LH_2 releases are proposed in this document. They will be extracted and expressed in concise language to be used as recommendations for RCS.

Abbreviations

BLEVE	Boiling Liquid Expanding Vapour Explosion
BOS	Background Oriented Schlieren
BSI	British Standards Institute
CFD	Computational Fluid Dynamics
CO_2/LCO_2	Carbon dioxide/liquid carbon dioxide
DEM	Delayed Equilibrium Model
DDT	Deflagration to Detonation Transition
DNV	Det Norske Veritas
DO	Discrete Ordinates
EDC	Eddy Dissipation Concept
FA	Flame acceleration
GH_2/LH_2	Gaseous/Liquid Hydrogen
GN_2/LN_2	Gaseous/Liquid Nitrogen
GO_2/LO_2	Gaseous/Liquid Oxygen
H/H_2	Hydrogen
HEM	Homogeneous Equilibrium Model
HFE	Helmholtz Free Energy
HNEM	Homogeneous Non-Equilibrium Mixture
HRM	Homogeneous Relaxation Model
HSL	Health and Safety Laboratory
H_2O	Water
INERIS	Institut National de l'Environnement industriel et des Risques
KIT	Karlsruhe Institute of Technology
LES	Large Eddy Simulation
LFL	Lower Flammability Limit
LHe	Liquid helium
LNG	Liquefied Natural Gas
MIE	Minimum Ignition Energy
NCSRD	National Centre for Scientific Research "Demokritos"
NIST	National Institute of Standards and Technology
N_2	Nitrogen

O_2	Oxygen
PPP	Pressure Peaking Phenomenon
PS	Pro Science
PSV	Pressure Safety Valve
RANS	Reynolds-averaged Navier Stokes
RCS	Regulations, Codes and Standards
RH	Relative humidity
RPT	Rapid Phase Transition
SNL	Sandia National Laboratory
TNO	Netherlands Organisation for Applied Scientific Research
TPRD	Temperature Pressure Relief Device
UFL	Upper Flammability Limit
UU	Ulster University
UVCE	Unconfined Vapour Cloud Explosion
WP	Work Package

Table of Contents

1 Introduction

The objective of this document is to provide easy to use guidelines to engineers for the safe design and operation of LH_2 infrastructure.

The PRESLHY project is a pre-normative project investigating knowledge gaps related to the use of liquid hydrogen in new applications. Three main topics were addressed:

- Cryogenic hydrogen release and dispersion,
- Ignition of cryogenic hydrogen mixtures,
- Combustion of cryogenic hydrogen.

These topics were studied through:

- A review of the existing state of the art and a ranking of the identified phenomena,
- A large experimental program covering the prioritized phenomena,
- The evaluation and validation of analytical and numerical approaches to assess these phenomena.

General rules, best practices and new means to assess the consequences of LH_2 releases are proposed in this document.

2 Terms and definitions

Auto-ignition temperature: the temperature at which spontaneous combustion will occur.

Boiling point: temperature at which the vapour pressure of a liquid equals the pressure surrounding the liquid and the liquid changes into vapour.

3 PRESLHY project contributions

3.1 Introduction to LH_2 specific hazards

3.1.1 Safety objectives of LH_2 use

There are three generic safety objectives for any system used in the industry:

- Protection of life,
- Protection of property,
- Protection of the environment.

Liquid hydrogen is a substance that has been used for decades in large industries and safety measures are in place for the protection of workers. However, the future LH_2 operations using LH_2 as an energy carrier in non-industrial settings and applications include working in environments close to the public whether it is refilling stations for cars or bunkering facilities for boats. The current perception of planned LH_2 operations and facilities is that they present an unacceptable risk to the public.

The first priority is the protection of life; it includes site workers, customers and the general public as well as first responders. The harm criteria for humans and infrastructure are presented in Appendix 1.

Facility owners should also consider reducing the damage of infrastructure and equipment and minimise disruption of business, preserve the corporate image and reduce direct and indirect financial losses. Attention should be paid to preventing the escalating effects of objects, events and layouts on damages and to value property in and around a facility (Saffers and Molkov, 2014).

Local authorities and regulators should be involved in the estimation of environmental impact from accidents involving hydrogen for:

- Prevention of significant damage to neighbouring facilities and reduction of domino effects,
- Limit adverse effects on the natural environment, such as asphyxiation and cold burns on fauna and flora.

3.1.2 Physical properties of GH_2 and LH_2

Hydrogen is the smallest chemical element and the most abundant chemical element in the universe. Its symbol is H. What is meant by gaseous hydrogen or hydrogen in the following document is the molecule H_2, dihydrogen.

3.1.2.1 GH_2 properties and associated hazards

Hydrogen is the lightest gas, being 14 times lighter than air. At normal conditions (standard pressure and temperature), hydrogen is an odourless, invisible, tasteless, non-corrosive and non-toxic highly flammable gas. Although it is not toxic, it is asphyxiant. It has a very low density, about 0.08 kg/m^3. However, the energy density of hydrogen is very high; 1 kg of

hydrogen contains approximately 2.5 times more energy than 1 kg of natural gas. Its flame emits ultraviolet light and is almost invisible to the naked eye.

There are two spin isomers of hydrogen: ortho-hydrogen molecules have a parallel arrangement of the nuclear spin of the two atoms and para-hydrogen ones have an antiparallel arrangement. At normal pressure and temperature, hydrogen gas is a mixture of ortho- (75%) and para-forms (25%).

Properties	Numerical values
Lower Heating Value	119.9 $kJ.g^{-1}$
Higher Heating Value	141.1 $kJ.g^{-1}$
Gaseous density at 273 K	0.0899 $kg.Nm^{-3}$
Specific heat (C_p at 273 K)	14199 $J.kg^{-1}.K^{-1}$
Specific heat ratio (at 273 K)	1.4
Diffusion coefficient in air	0.61 $cm^2.s^{-1}$
Minimal ignition energy	20 µJ
Flammability range in air	4 -75% vol
Detonation range in air	13 - 65% vol
Flame velocity in air	260 $cm.s^{-1}$
Detonation velocity in air	2 $km.s^{-1}$

Figure 1: Thermo-physical properties of gaseous hydrogen.

Regarding the properties given in Figure 1, the associated behaviours for hydrogen are the following:

- Low density
  - H_2 rises and disperses rapidly (lighter than air),
  - Quick dispersion in free space after stopping the release,
  - Accumulation in the highest locations, close to the enclosure roof in confined spaces,
  - High pressure required to store large amounts in the gaseous state.
- High diffusivity

  Concentration will become totally homogeneous in a confined space after stopping release without external disturbance.
- Low viscosity

  Tendency to leak.
- Combustible with a large flammable range and low ignition energy required

  High potential for fire or explosion (deflagration).
- Radiative properties

  Less radiative than methane and other combustible compounds. However, for large release rate (1 – 7 kg/s), hydrogen radiative fraction is comparable to natural gas.

Hazards associated with GH_2

Like all fuels, precautions are necessary for the safe handling and use of hydrogen. Potential hazardous events are the release of hydrogen, ignition of the hydrogen-air flammable mixture, the burst of pressurized vessels…

- **Hydrogen release in free field**

Two main scenarios can occur in that case:

- Release with immediate ignition: the released hydrogen immediately ignites and burns. A jet fire forms as long as the hydrogen source is not shut off. The hydrogen flame from a highly pressurised storage can cover distances of tens of meters and cause life-threatening conditions by the flame itself and thermal radiation (depending on the exposure duration).

- Release with delayed ignition: if the ignition of a highly turbulent flammable jet is delayed, pressure loads must be considered along with the above-mentioned thermal hazards. Depending on the scenario, i.e. release duration and ignition delay time, a flammable cloud has the potential to form before ignition. The ignition of this cloud will induce a deflagration (UVCE: unconfined vapour cloud explosion). The level of congestion (presence of obstacles) can be an escalating factor and leads to a risk of deflagration to detonation transition (DDT).

- **Hydrogen release in confined spaces**

A hydrogen release in a confined space can result in the accumulation of hydrogen. In practice, what is referred to as a confined space here can be a container hosting process or hydrogen storage, garages, parking, tunnels, etc.

The hazards include:

- The destruction of the structure, enclosure or building by pressure peaking phenomena during unignited release,
- The formation of a flammable mixture that can potentially combust if ignited,
- Asphyxiation resulting from the displacement of breathable air by hydrogen (oxygen depletion).

- **Pressure peaking phenomenon**

Pressure peaking is a phenomenon observed for gases lighter than air. It can result in overpressure exceeding the enclosure or building structural strength limit in case of a sufficiently high hydrogen release rate and low ventilation rate. The enclosure can be strongly damaged up to total destruction.

In order for the pressure peaking to occur, the hydrogen release flow rate should be sufficiently high to result in complete displacement of air from the enclosure, i.e. the hydrogen concentration within the enclosure must reach 100%. This phenomenon was theoretically and experimentally investigated in the Hyindoor project and other studies. The main conclusion was that the pressure peaking phenomenon (PPP) is a complex

combination of the following parameters: high release flow rate, small size enclosure and small size of vents.

- **Hydrogen build-up**

Hydrogen released in a confined space will accumulate. However, the concentration level and distribution will be different based on the ventilation rate in the considered enclosure. Three cases are considered and briefly discussed hereafter.

  - No ventilation

The enclosure is fully closed, the concentration inside the enclosure will depend on the release duration and can reach 100%.

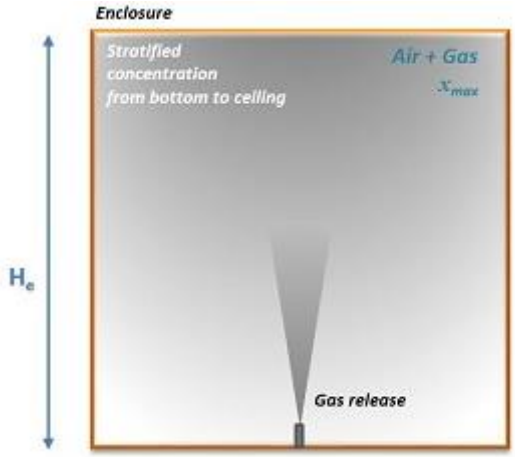

Figure 2: hydrogen gaseous release in an enclosure without ventilation.

  - Natural ventilation

Natural ventilation is driven by the buoyancy effects created by the released hydrogen inside an enclosure with ventilation apertures and limiting hydrogen concentration. Two regimes are then identified: a mixing regime and a displacement regime, depending on the placement of the various apertures.

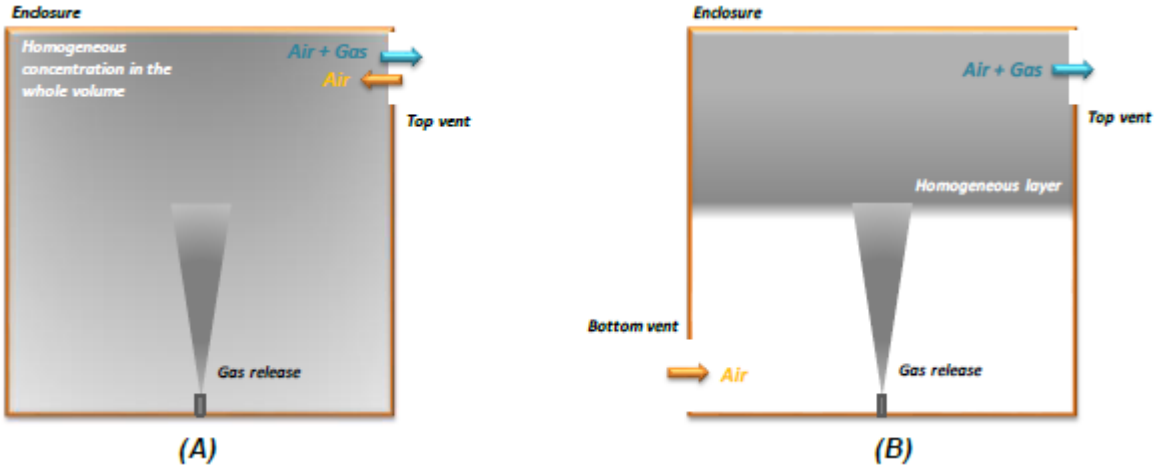

Figure 3: Hydrogen gaseous release inside a naturally ventilated enclosure. (A) Mixing regime, (B) displacement regime.

Natural ventilation is a way of mitigating hydrogen build-up in case of accidental release in a confined space.

- Mechanical ventilation

Mechanical ventilation is driven by fans or other mechanical devices, limiting hydrogen concentration inside a confined space. It is a way of mitigating hydrogen build-up in case of an accidental release in a confined space. It can be used when natural ventilation is not possible or not sufficient to reach safety targets.

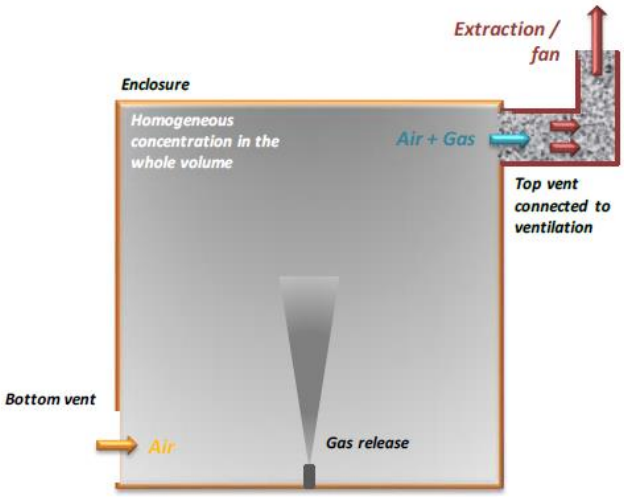

Figure 4: Hydrogen gaseous release inside a mechanically ventilated enclosure.

- **Vented explosion**

If a hydrogen cloud, with a sufficient volume, reaches its flammable range within a confined space (between 4 and 75% H_2 at 20°C), an explosion can occur in case of delayed ignition of the flammable mixture. The overpressure generated by the flame acceleration can lead to the destruction of the enclosure but can be limited with dedicated explosion panels.

Figure 5: Hydrogen confined explosion with and without venting disposal. Experiments performed in HySEA project.

Figure 5 illustrates the efficiency of venting panels in the case of a hydrogen explosion inside a container. The third illustration line shows how the presence of panels allows avoiding the destruction of the container and projection of fragments. Thanks to the explosion panels on the roof, the flames are directed upwards and the container deformation is limited.

Venting panels are mitigation means allowing limiting the effect of an explosion in a confined space. It should be noted that for the more reactive hydrogen mixture (>25 % vol.), the ability to vent successfully the explosion needs very careful design, in particular if the space is congested, since the speed of pressure development is such that vent panels may not fail fast enough, especially if conditions are such that a deflagration to detonation transition happens.

- **Burst of pressurized vessel**

The burst of a pressurized vessel is a physical explosion.

The resistance of a vessel can be degraded, for various reasons e.g. presence of a continuous and established fire inducing a loss of containment of the stored hydrogen with a rapid expansion generating overpressure wave, fireball and potential fragments. These may cause injuries and fatalities as well as structural damages.

A burst can occur at various conditions:

- At normal operating pressure due to:
  - Degradation with the time of the pressurized vessel (e.g. corrosion),
  - Mechanical impact(s) on the pressurized vessel,
- At 'bursting' pressure (rupture pressure) due to:
  - Overfilling,
  - Inadequate pressure relief,
  - Other events such as internal explosion or reaction, fire aggression...

- **Oxygen depletion**

A large release of hydrogen will displace the ambient air, causing oxygen depletion especially in confined spaces such as instrument cabinets or process containers. An oxygen-deficient atmosphere can lead to unconsciousness up to death.

Oxygen percent at sea level (atmospheric pressure = 760 mmHg)	Effects
20.9	Normal (below 19.5% is considered oxygen deficient)
19.5 – 10	Increased breathing rates; accelerated heartbeat; and impaired attention, thinking, and coordination
10 – 6	Nausea, vomiting, lethargic movements, and perhaps unconsciousness
<6	Convulsions, then cessation of breathing, followed by cardiac standstill (death). These symptoms can occur immediately.

Figure 6: Effects of various oxygen concentrations on human health.

- **Cuts of skin and protective clothing**

High-pressure hydrogen jets can cut bare skin or other tissue. The releases of pressurised hydrogen even from a small leak may penetrate a person's skin. Protective clothing may not prevent skin damage.

3.1.2.2 LH_2 properties and associated hazards

The following phase diagram shows the phase behaviour of hydrogen under different conditions of pressure and temperature.

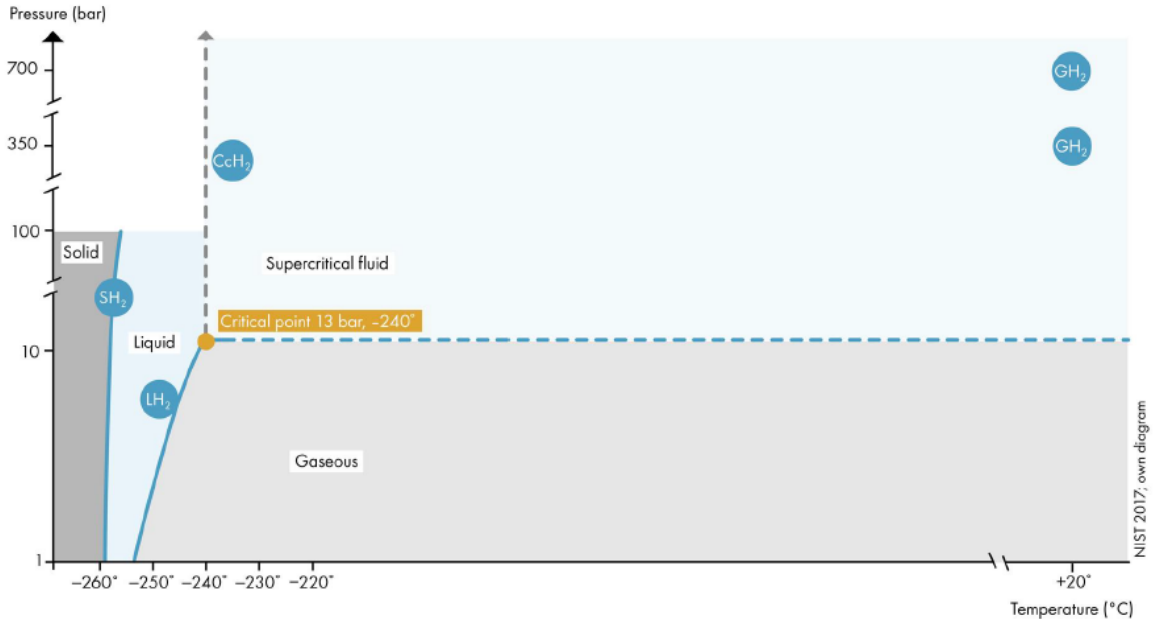

Figure 7: Hydrogen phase diagram (NIST, 2017).

Liquid hydrogen (LH_2) is a clear cryogenic liquid with a light blue tint, odourless and non-corrosive with a normal boiling point at -252.87°C (20.28 K) at atmospheric pressure. Liquid hydrogen at 20 K is composed of 99.8% para-hydrogen. At its boiling point, the density of LH_2 is about 71 kg/m^3.

Regarding the properties of LH_2, the associated behaviours for liquid hydrogen are the following:

- Low boiling point
  - Cryogenic liquids are liquefied gases that are kept in their liquid state at very low temperatures,
  - For storage, highly insulated vessels are required to maintain the low temperatures (perlite or multi-layer insulation technology),
  - In poorly insulated containers, some cryogenic liquids actually condense the surrounding air, forming a liquid air mixture.
- State at normal temperatures and pressures

  All cryogenic liquids are extremely cold and are gases at normal temperatures and pressures.
- High density

Small amounts of liquid can expand into very large volumes of gas.

- Vaporization of cryogenic liquids

  The vapours and gases released from cryogenic liquids also remain very cold. They often condense the moisture in the air, creating a highly visible fog. They can also potentially liquefy and/or solidify components of air (O_2, N_2).

- Flammable properties
  - By extrapolating data from Figure 8, showing the influence of temperature on the flammability limits of hydrogen, the flammable range of cold gas is narrower than hydrogen gas at higher temperatures. Indeed, the lower flammability limit is increased and the upper flammability limit is decreased for low temperatures.
  - Minimum ignition energy is slightly higher for cold gases compared to gases at ambient temperatures.

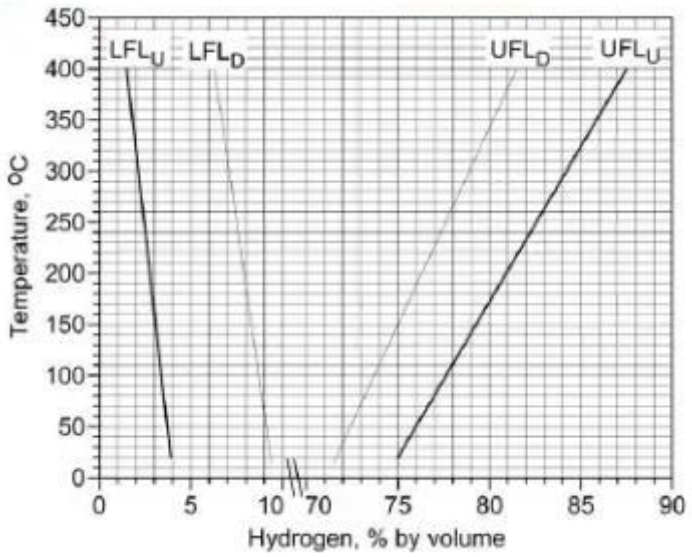

Figure 8: LFL and UFL for hydrogen-air mixtures as a function of temperature. Black lines - upward flame propagation (Schroder and Holtappels, 2005); grey lines - downward flame propagation (Coward and Jones, 1952).

Hazards associated with LH_2

- **Pressurized LH_2 release**

Similarly to the GH_2 release, there are two scenarios to be considered:

- Immediate ignition: it seems that the immediate ignition of a LH_2 high-pressure jet is similar to a GH_2 high-pressure jet, with overpressure effects due to ignition.
- Delayed ignition: the higher density of the saturated hydrogen vapour at low temperatures may cause the hydrogen to flow horizontally or downwards after the immediate release of liquid hydrogen (heavy gas behaviour). Usually, the condensation of atmospheric humidity will also add water to the mixture cloud (making it visible) making it even denser.

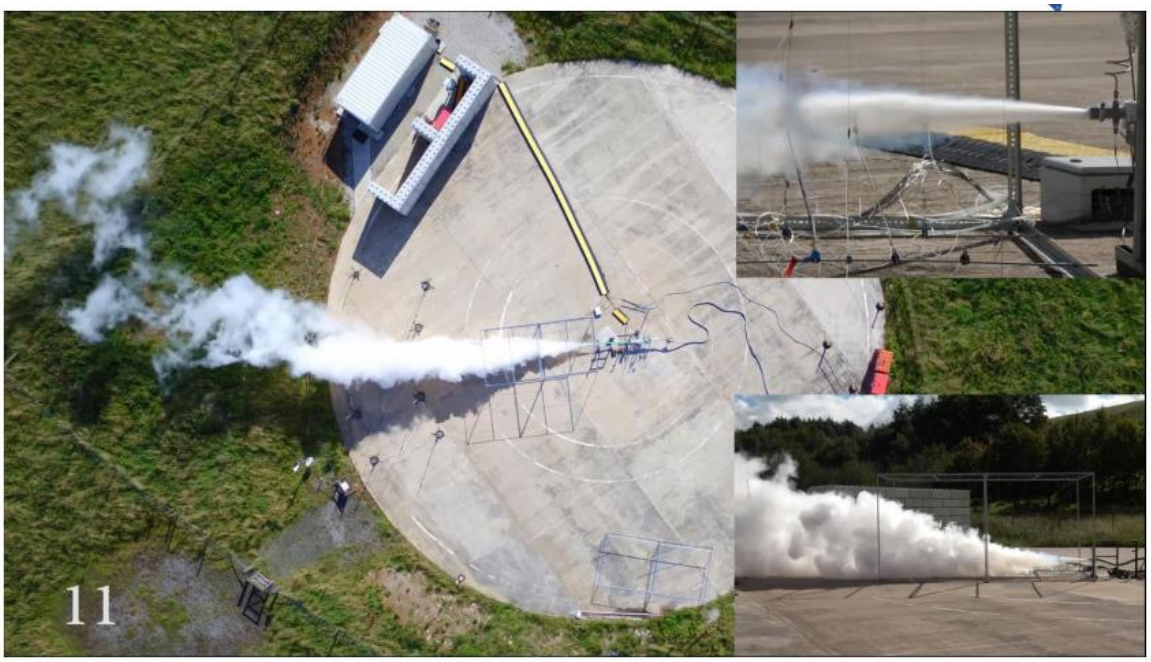

Figure 9: LH_2 large-scale release (HSE, test realized within PRESLHY).

Due to liquid high density and vaporization at ambient temperature, the flammable cloud is significantly larger than the cloud induced by a gaseous hydrogen release. Therefore, consequences in the case of ignition of this flammable cloud are more important in terms of intensity and distance of effects.

If the pressure is low enough, in some conditions, in addition to the hydrogen jet, a rainout phenomenon could be observed, i.e. the formation of hydrogen droplets falling on the ground forming a hydrogen pool. In these cases, it is difficult to know which phenomenon - between jet or pool- will induce the most important consequence in case of ignition or what will be the consequence of the combination of these two physical phenomena.

The formation of hydrogen pools was also observed for vertical releases pointing downwards.

- **Cryogenic LH_2 pool**

A LH_2 spillage can induce the formation of a pool. LH_2 will vaporize and form a flammable cloud with a significant volume.

Weather conditions have a significant impact on the propagation and dispersion of the cloud. Small-scale experiments by KIT showed no spontaneous ignition of the hydrogen liquid pool. However, forced ignition of the pool highlighted the importance of the ground on the deflagration effects. Sand and concrete induce the same behaviour but gravels escalate consequences.

- **UVCE**

In the case of a LH_2 spillage on an industrial site, a cold and reactive H_2/air cloud could be formed. In the case of ignition, the flame could interact with various obstacles (vaporizers,

pipe rack, vegetation) possibly leading to flame acceleration and even DDT in the worst-case scenario.

- **BLEVE**

A BLEVE or Boiling Liquid Expanding Vapour Explosion is an event associated with the catastrophic failure of a pressure vessel containing a liquid stored at a temperature above its saturation temperature at atmospheric pressure. On failure, some of the liquid will flash to vapour resulting in the generation of overpressure; ignition of the released contents produces a large fireball that can determine the hazard range. This hazard is thus relevant to LH_2, which although stored cryogenically, is also at modest pressure. LH_2 vessels are designed to relieve safely in the event of loss of the insulating vacuum, however, failure/blockage of this system could lead to a BLEVE, or a fire attack could raise the pressure and lead to a BLEVE with a fireball due to inadequate venting of pressure. It is worth noting that in LNG tests, the tank insulation material appeared to delay or prevent any BLEVE if the pressure relief occurs safely; and for unprotected vessels (LPG) BLEVE can happen even if the pressure relief occurs.

LH_2 BLEVEs are being investigated experimentally in the SH2IFT project. They are planned for Q3/Q4 2021.

- **RPT**

RPT or Rapid Phase Transition is a "cold" or physical explosion. This is a known phenomenon for LNG in particular. The cryogenic liquid vaporizes violently upon coming in contact with water causing a cold explosion, there is no combustion.

In theory, there are three types of RPT:

- Spontaneous,
- Delayed,
- Triggered.

Based on the theories and mechanisms for RPT (see Figure 10), it is unlikely a spontaneous RPT will happen for LH_2-water. However, the possibility to provoke an early or delayed RPT by external triggering (waves) or an early spontaneous RPT by high-momentum injection of LH_2 into/onto water cannot be excluded.

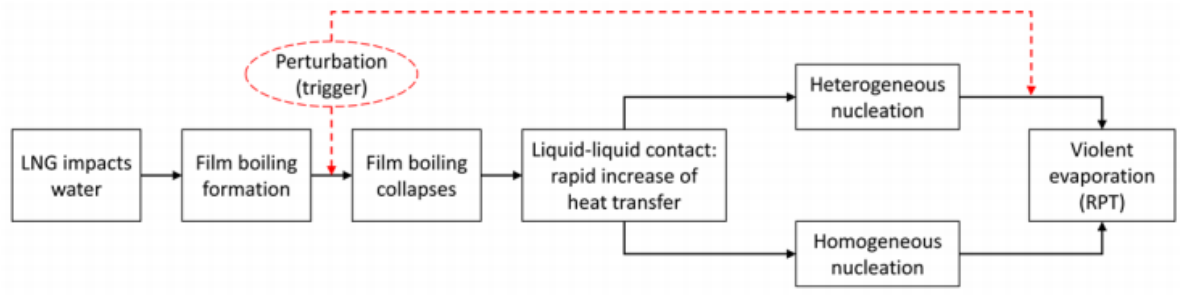

Figure 10: RPT mechanism for LNG.

This will be investigated by experiments performed in the SH2IFT project, planned for Q3/4 2021.

- **Cryogenic hazards**
    - Material embrittlement

Cryogenic temperatures on materials can reduce the strength of structures to irreversible failures. It is a critical factor for metals under stress.

    - Liquefaction/solidification of air components

In the case of LH_2 or cold GH_2 releases, it is possible that solid or liquid particles (water, CO_2 freezing) and/or LH_2 droplets and air-condensate droplets (friction and break-up) may ignite. Ignition of these droplets was not observed within PRESLHY but droplets were identified in releases.

    - Extreme cold hazard

Cryogenic liquids and their associated cold vapours and gases can produce effects on the skin similar to a thermal burn. Brief exposures that would not affect the skin on the face or hands can damage more delicate tissues such as the eyes. Prolonged exposure of the skin or contact with cold surfaces can cause frostbite. The skin appears waxy yellow; there is no initial pain but an intense pain when frozen tissue thaws.

Unprotected skin can stick to metal that is cooled by cryogenic liquids. The skin can then tear when pulled away. Even non-metallic materials are dangerous to touch at low temperatures. Prolonged breathing of extremely cold air may damage the lungs.

    - Asphyxiation

When cryogenic liquids form a gas, the gas is very cold and usually heavier than air. This cold, heavy gas does not disperse very well and can accumulate near the floor. Even if the gas is non-toxic, it displaces air. When there is not enough air or oxygen, asphyxiation and death can occur. Oxygen deficiency is a serious hazard in enclosed or confined spaces.

Small amounts of liquid can evaporate into very large volumes of gas. In the case of hydrogen, one litre of LH_2 vaporizes to 848 litres of GH_2 when warmed to room temperature.

3.1.3 LH_2 refilling station: description

The LH_2-based refuelling station under consideration will be made of the following basic elements and is the base design used for the definition of accidental scenarios:

- A horizontal LH_2 tank ($22m^3$ - 1098 kg) with a maximum operating pressure of 10.3 bara;
- An insulated process line from the bottom of the storage to the LH_2 pump, driving LH_2 from the storage tank to the vaporizer. The LH_2 pump is able to pump LH_2 up to 1000 bar;
- A heater called VAP on the figure hereafter: hot oil or electric to heat up hydrogen at 1000 bar;

- A 1000 bar gaseous buffer of a few m^3. These buffers are usually bundles of type I or II metallic cylinders or long metallic tubes.

All the other parts such as the dispenser, filling hose etc. of the refuelling station are similar to classical GH_2 refuelling stations.

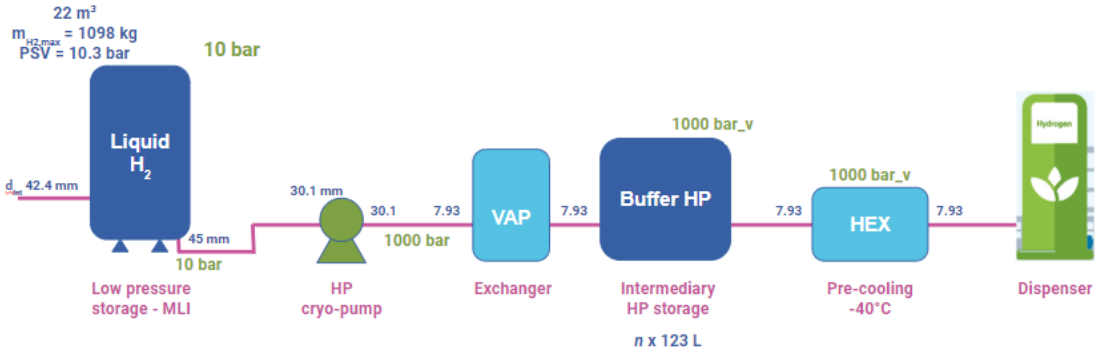

Figure 11: Simplified model of a liquid hydrogen refuelling station.

3.1.4 LH_2 refilling station: accidental scenarios considered

Due to liquid hydrogen characteristics and the requirements of hydrogen energy applications, liquid hydrogen used in confined configurations is not in the scope of the PRESLHY project.

The configuration under consideration is that of the LH_2-based fuelling station presented here before.

The main accidental scenarios suggested and considered within PRESLHY for this station are (this list is not exhaustive):

- Scenario 1: vessel burst at P < P(PSV); BLEVE.
- Scenario 2: vessel burst at P > P(PSV); flash fire.
- Scenario 3: full bore rupture of the pipe before the pump.
- Scenario 4: partial rupture of the pipe before the pump.
- Scenario 5: full bore rupture of the pipe after the pump.
- Scenario 6: partial rupture of the pipe after the pump.

Safety-relevant phenomena associated with incidents/accidents involving LH_2 systems and infrastructure are summarized in the diagram in Figure 12.

The event starts with a loss of containment of the LH_2 inventory. The loss of containment can take three shapes; it is either a vessel burst, an instantaneous release or a continuous release. Depending on if the released hydrogen ignites or not, immediately or with a delay, multiple scenarios are possible. The ignition can be caused by the presence of open fire, hot surface, electric or mechanical sparking and other factors, as well as the hydrogen-specific phenomenon of spontaneous ignition by diffusion (Molkov, 2012).

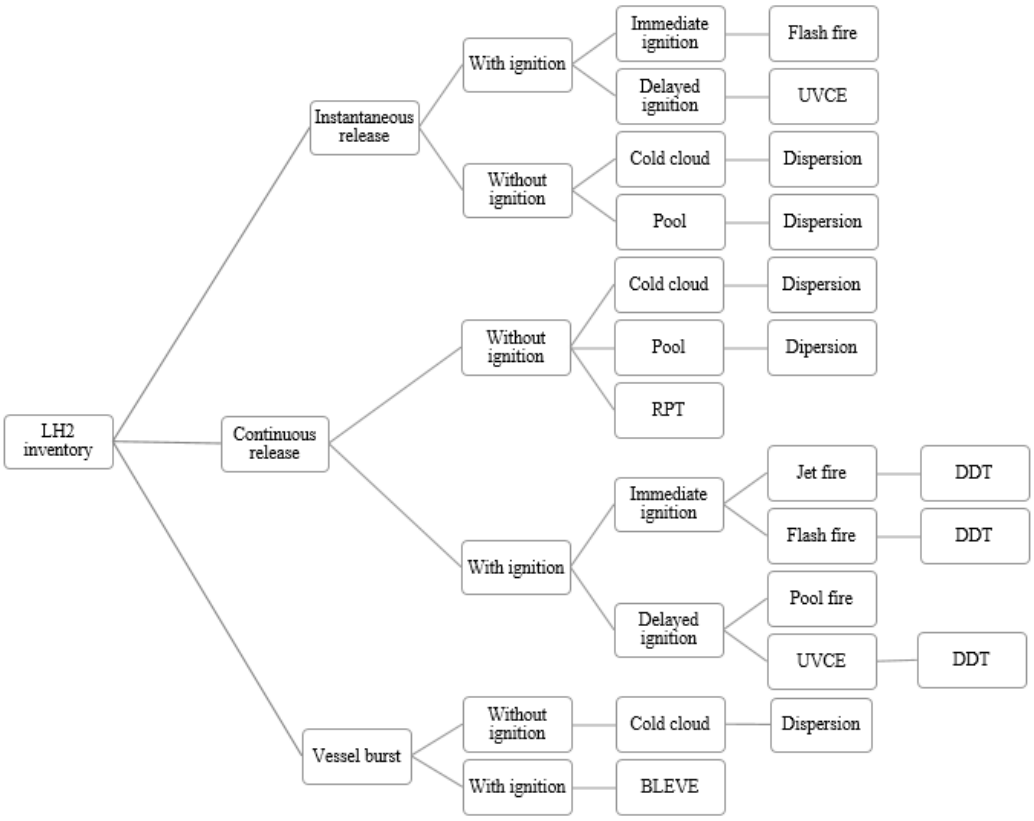

Figure 12: Phenomena diagram cascading from the loss of containment of LH_2 inventory.

If there is no ignition, three phenomena are identified: RPT, the formation and dispersion of a cold cloud, the formation of a pool and its dispersion.

If ignition has occurred, five distinct phenomena can happen: BLEVE, flash fire and jet fire if the ignition is immediate, UVCE and pool fire if the ignition is delayed.

3.2 Cryogenic hydrogen release and dispersion

3.2.1 Main outcomes from PRESLHY on cryogenic releases

More details about the experiment setups can be found in the deliverable D2.6 "Refined Work Program". More details about the experimental results can be found in D3.3 "Experimental investigation of cryogenic hydrogen release and dispersion".

3.2.1.1 Small scale cryogenic H_2 and multiphase releases

KIT/PS led two sets of experiments to investigate transient multiphase H_2 releases from pressurized vessels. Tests were made at ambient (300 K) and cryogenic temperature (80 K) on small scale using the DISCHA facility (2.8 dm^3) and at ambient and cryogenic temperature with LH_2 (20 K) on the medium scale using a cryo-vessel (225 dm^3).

In the DISCHA tests, the initial pressure varied from 5 to 200 barg and the nozzle cross-section from 0.5 to 4 mm. In the cryo-vessel, the initial pressure varied from 2 to 5 bars with a nozzle cross-section of 2 or 4 mm. For both sets of experiments, the pressure and temperature were monitored inside the vessel. Outside the vessel, the temperature and H_2 concentration were measured alongside optical monitoring with Background oriented Schlieren (BOS), photo and videography.

For large diameters in the cryo-vessel, and large diameters and high pressure in DISCHA, a huge fraction of entrained particles in the jet was observed. In addition, in the cryo-vessel, 'finger-like' structures formed at the nozzle due to the freezing of moisture/air contents.

3.2.1.2 LH_2 pool formation and evaporation

KIT investigated the formation and evaporation of pools of LH_2 on various substrates: concrete, water, sand and gravel. The temperature was monitored in the substrate, in and above the pool. The concentration of H_2 was measured above the pool. Optical instrumentation was used to study the phenomenon: photo, video and thermal camera.

They observed pool formation above all substrates but the increasing porosity tended to delay the pool formation. Indeed, in these cases, the increased porosity meant an increase in surface so an increase in vaporization rate which delayed the pool formation.

3.2.1.3 Large scale liquid and multiphase releases

HSL performed 25 unignited LH_2 releases through 6, 12 and 24.4 mm nozzles with an indicated tanker delivery pressure of 1 or 5 bar and release heights of 0.5 and 1.5 m. The discharge flow rates were monitored as well as the near field dispersion. It was observed that rainout did not occur during the established flow of these releases but cannot be ruled out as a credible hazard for LH_2 spills with different initial conditions. Pools were able to form with vertically downwards releases only. Solid deposits formed around the release point and on impingements on the sensors.

3.2.2 Consequence assessment: an analytical and numerical approach

More details about the analytical and numerical results and approaches can be found hereafter in the appendixes, in D3.2 "Computational investigation of cryogenic hydrogen release and dispersion" and D6.5 "Detailed description of novel engineering tools for LH_2 safety".

3.2.2.1 Concentration decay in jets

UU tested the similarity law by Chen and Rodi (1980) for concentration decay in momentum-dominated hydrogen jets released at cryogenic temperature.

Analysis showed that cryogenic hydrogen jets follow the same decay trend as ambient temperature releases, therefore it is considered that similar considerations may be applied (see Saffers and Molkov, 2013; Cirrone *et al*., 2019).

The similarity law could be used to estimate the distance from the nozzle where a concentration of interest is reached in free field (without interaction with the ground or obstacles). For instance, the location of LFL to determine the axial size of the produced flammable envelope and, hence, provide guidance on equipment location or site layout to satisfy hazard distances. The tool description and validation range is presented in more detail in Annex 2.3

3.2.2.2 Storage tank blowdown

Heat transfer through a tank wall should be taken into account in the modelling of transient hydrogen releases during blowdown. Heat transfer through a tank wall can affect the gas temperature dynamics during a tank blowdown (see Schefer *et al.*, 2007), and thus affect hydrogen properties at the nozzle and duration of a release.

Effect of heat transfer may further increase in the case of cryo-compressed storage tanks with damaged insulation, resulting in different thermodynamic conditions in the storage and at the nozzle compared to a case approaching the adiabatic limit, and possibly even determining if the flow will be gaseous or multiphase.

UU developed a non-adiabatic blowdown model for transient cryogenic and ambient temperature releases by taking into account the heat transfer through the storage tank and release piping system walls (PRESLHY D6.5). The model accurately predicts the pressure and temperature dynamics during blowdown for releases with diameter in the range 0.5-4 mm, initial pressure up to 200 bar and initial temperature of 80 K and 300 K.

3.2.2.3 DISCHA tool, for physical properties and discharge calculations

NCSRD developed an engineering tool for cryogenic and ambient release calculations. The DISCHA tool can be applied to calculate accurate physical properties of pure substances

and perform discharge calculations either in transient (blowdown) or in steady-state mode with account of discharge line effects (friction, area change, extra resistance due to fittings and heat transfer through pipe walls). Stagnation conditions are either assumed adiabatic or provided as input. Single-phase physical properties are calculated using the HFE formulation. Phase distribution is calculated with HEM or various HNEM models. The tool was validated against a series of steady and transient release experiments either pre-existing or performed within PRESLHY, see deliverable D3.2.

The NCSRD release modelling investigations led to the following conclusions:

- The distribution of flow parameters (pressure, temperature, velocity, etc.) along the discharge line for under-expanded releases depends strongly on the type of discharge line rupture. For full-bore rupture, flow parameters continuously change along the line towards its exit. For partial bore rupture (or nozzle) with a diameter less than half that of the preceding line, flow parameters are nearly constant over most part of the discharge line and all the significant changes occur near the exit. In the first case, discharge line friction plays an important role in controlling the mass flow rate. In the second case, flow velocities are relatively small along the line and strongly increase near the exit, thus the mass flow rate is controlled by the characteristics of the exit nozzle rather than any line resistance before the nozzle area.
- Special attention should be given to account for flexible pipeline flow resistance in experiments and the design of hydrogen applications as flexible lines can experience up to 10 times larger flow resistances than rigid lines.
- Mass flow rates during blowdown are systematically enhanced by non-adiabatic tank effects and systematically reduced primarily by discharge line resistance (friction, extra resistance due to fittings) and to a lesser or much lesser extent by discharge line heat transfer. These opposing effects may balance each other and justify the use of simpler modelling, i.e. assuming an adiabatic tank, neglecting the discharge line and using a discharge coefficient of 1.0. Indeed, this simple approach was observed to acceptably reproduce released hydrogen mass time histories compared to experimental data for most of the gaseous (cryogenic or ambient) hydrogen blowdown cases considered, although it suffers from an underestimation of exit temperatures. These phenomena need to be further investigated with new dedicated experiments, where special attention should be given to parameters affecting resistance and heat transfer.

For two-phase releases, HEM model performance can be significantly improved if more accurate information is provided as input regarding stagnation conditions and discharge line resistances. Still, non-equilibrium effects need to be taken into account below the liquid-vapour saturation curve and HNEM models (like HRM and DEM) need to be extended to hydrogen, based on new dedicated experiments.

3.2.2.4 Spreading rate of cryogenic pools

The purpose of this model is to estimate the size of the liquid pool on the ground produced by a low-pressure spillage of liquid hydrogen.

HyPond is a single algebraic formula to estimate the maximum extent of the liquid pool likely to spread on the ground following a low-pressure spillage of liquid hydrogen. Maximum extent refers to a free expansion of the pool over a flat, free of obstacles and horizontal surface. Since in such a model the vaporization rate is equal to the feeding rate of the pool, the tool may help to decide if a retention basin could be useful to reduce the vaporization rate and the size of the dangerous cloud.

A quiet boiling regime is assumed which is in place 10-20 s after the start of the spill. Therefore, the present model applies rigorously only to prolonged spills and should not be used for catastrophic ruptures leading to very short release durations. The tool description and validation range are presented in more detail in Annex 2.5.

3.2.2.5 Method to calculate the final state when mixing LH_2 and moist air

The purpose of this model is to determine the thermodynamic state when LH_2 is mixed with ambient air. The final state is defined by temperature, hydrogen volume fraction and density.

The primary use of such an analysis is to support experiments on dispersing clouds of cold hydrogen in circumstances where there is a minimal exchange of heat except with entrained air. The method allows estimation of gas concentrations from measured temperature if the humidity and temperature of ambient air are known. The method is valid for final temperatures sufficient to prevent condensation of oxygen or nitrogen. This starts to occur at final temperatures below about 72 K. This limiting temperature corresponds to a final hydrogen volume fraction of 70-80% depending on atmospheric temperature and relative humidity (RH).

3.2.2.6 CFD work

- UU performed a CFD study to analyse the cryogenic hydrogen flow in a release pipe and assess the effect of conjugate heat transfer through the pipe walls. The simulated mass flow rates were compared against experimental measurements in tests performed by KIT in the ICEFUEL project for releases with storage pressure from 3 to 20 bar, the temperature of 80K and nozzle diameter from 2 to 4 mm (Cirrone *et al*., 2021).

– Simulations showed that conjugate heat transfer through a pipe wall can greatly affect the hydrogen flow parameters and should be included in modelling to reproduce the experimental mass flow rate and characteristics of the resulting jet.
– CFD modelling could be applied to assess the effect of conjugate heat transfer through a pipe wall on a cryogenic hydrogen flow and accurately predict hydrogen parameters at the nozzle.
– LES CFD approach with a density-based explicit solver can be used for modelling of hydrogen flow in a pipe.

- NCSRD performed CFD modelling investigations to validate their tool for cryogenic dispersion and BLEVE. It led to the following conclusions:

– ADREA-HF CFD code was validated against a variety of cryogenic dispersion experiments (large-scale steady LH_2 and LHe releases, steady-state and transient cryogenic gaseous H_2 releases).
– ADREA-HF CFD code was validated against LCO_2 BLEVE experiments and used to perform a parametric study based on the pre-existing BMW BLEVE experiments.

- A CFD inter-comparison work for gaseous cryogenic under-expanded hydrogen blowdown releases was done using the experiments performed by Sandia National Laboratories (SNL) and described in Hecht and Panda (2019). Two tests were selected with 1 mm nozzle, with stagnation conditions 2 bara, 58 K and 5 bara, 50 K and two tests with 1.25 mm nozzle, with stagnation conditions 2 bara, 61 K and 4 bara, 54K. During these experiments, a low-intensity co-flow of air (0.3 m/s) was applied around the jet to minimize the effect of any other room currents. Most participants of this benchmark got numerical results in close agreement with the experiments.

- A CFD inter-comparison work was done based on the DISCHA experiments performed by PS and KIT within PRESLHY. The test selected involved blowdown of hydrogen from a 2.815 dm^3 tank at 200 bar, 77 K stagnation conditions through a 4 mm nozzle, see Friedrich *et al.* (2019) and Veser *et al*. (2021). The benchmark led to the following conclusions:

– Measuring arrival time and concentration decay rate close to the source for transient under-expanded hydrogen jets is a big challenge and needs further future research supported by simulations;
– It is suggested for future experiments near the source to a) reduce the length of the plastic tube extracting hydrogen/air mixtures from the nominal sensor location as much as possible and b) use collocated temperature sensors at nominal sensor locations in order to derive hydrogen concentration, using the adiabatic mixing approach.

3.2.3 Summary

Experiments

The issues addressed in the experimental part of WP3 were the characterization of the discharge coefficients of pressurized cryogenic releases and LH_2 releases at a small and large scale, and the formation of a LH_2 pool from a release (rainout, delays, and evaporation). The main observations are:

- For both small and large-scale hydrogen releases, solid deposits formed at the nozzle likely due to freezing of moisture/air contents and on impingement on sensors. In the small-scale releases, large diameters lead to a high fraction of entrained particles in the jet.
- Pool formation occurred on all substrates tested. With increasing porosity of the substrate, a delay in the pool formation occurred.

- For an established flow of horizontal releases, no rainout was observed and pools formed for vertically downward releases. However, at this time, it is advised not to rule out rainout as a credible hazard for LH_2 spills since different initial conditions could lead to a different outcome.

Analytical tools

- Cryogenic hydrogen jets follow the same decay trend as ambient temperature hydrogen releases; hence, the similarity law can be used to estimate the distance from the nozzle where a concentration of interest is reached, e.g. the location of LFL.
- The non-adiabatic blowdown model for a hydrogen storage tank can be used to accurately predict the pressure and temperature dynamics during blowdown for transient cryogenic and ambient temperature releases.
- The release model can be used to predict the mass flow rate generated by a full bore or partial rupture of a pipe for cryogenic and ambient temperature releases. The tool takes into account discharge line effects (friction, area change, extra resistance due to fittings and heat transfer through pipe walls), stagnation conditions and single or two-phase releases. The release modelling investigations led to the following conclusion:
    - Special attention should be given to account for flexible pipeline flow resistance in the design of hydrogen applications as flexible lines can experience larger flow resistances than rigid lines;
    - New dedicated experiments are necessary to investigate the influence of parameters affecting resistance and heat transfer in the pipe.
- HyPond can be used to estimate the size of the liquid pool on the ground produced by a low-pressure spillage of liquid hydrogen. It applies for prolonged spills ($t > 20s$) over a flat, free of obstacles and horizontal surface.
- The last method allows us to determine the thermodynamic state when LH_2 is mixed with ambient air. The final state is defined by temperature, hydrogen volume fraction and density. The method allows estimation of gas concentrations from measured temperature if the humidity and temperature of ambient air are known and is valid for final temperatures sufficient to prevent condensation of oxygen or nitrogen.

Numerical tools

- LES CFD approach with a density-based explicit solver can be used for the modelling of cryogenic hydrogen flow in a pipe accounting for the effect of conjugate heat transfer through the pipe wall, and the estimation of the resulting mass flow rate.
- A CFD model (ADREA-HF) has been validated for cryogenic dispersion and BLEVE.

- A CFD inter-comparison work for gaseous cryogenic under-expanded hydrogen blowdown releases led to the conclusion that more experiments are necessary to fully understand the phenomena involved in the release and measure the variables (concentration decay, arrival time, temperature) close to the nozzle.

3.3 Ignition of cryogenic hydrogen

3.3.1 Main outcomes from PRESLHY on ignition of cryogenic hydrogen

More details about the experiment setups can be found in the deliverable D2.6 "Refined Work Program". More details about the experimental results can be found in D4.3 "Experimental investigation of ignition of premixed systems with cryogenic hydrogen".

3.3.1.1 Fundamental ignition parameters

Ignition temperature by hot surface was found to be independent of mixture temperature, while stoichiometry and flow velocity had a marginal influence.

Measurements of minimum ignition energy (MIE) by spark ignition successfully reproduced reference tests at ambient temperature. Tests for hydrogen-air mixtures at -100°C showed a slight increase in MIE.

3.3.1.2 Electrostatic ignition in cold jet

KIT investigated the electrostatic ignition of cold jets and plumes using the DISCHA experimental setup and the cryovessel, both described in section 4.2.1.1.

In both configurations, strong electrostatic fields were observed and no spontaneous ignition happened.

3.3.1.3 Electrostatic ignition in cold plume

The experiments done by HSL were designed to measure two distinct modes of charging:

- Charging due to charge separation near to the LH_2/pipe interface, monitored via the wall current from an electrically isolated section of pipework;
- Charging of the cloud generated by a jet.

The main trends observed during the experiments were as follows:

- The flow of LH_2 in pipes can cause electrostatic charges and certain conditions encourage it;
- Cryogenic hydrogen releases at relatively low pressures (maximum 5 barg) did not reliably generate an electric field under the conditions of the experiments.

From the plume measurements, it is clear that while a transient field can be measured, a charged plume forming from an established cryogenic jet is unlikely for the initial conditions of these experiments. From these trials, it is evident that the flow of LH_2 in pipes can cause electrostatic charges and that certain conditions encourage it. These findings could be used for either designing LH_2 pipework so that the development of two-phase flows is limited (through vacuum insulation for instance) or ensuring that the pipework contains no electrically isolated sections.

3.3.1.4 Ignition above a pool

KIT performed ignition above LH_2 pools on various substrates: concrete, water, sand and gravel, with different ignition positions and various LH_2 filling levels in the pool. The

different filling levels were necessary to provide for flammable H_2-concentrations in the region of the ignition position.

No spontaneous ignition was noted above the pool. The observed combustion behaviour of pools above concrete, water and sand is similar. Due to the high porosity in the gravel bed, other phenomena became dominant: e.g. accumulation of frozen air components in the bed. The ignition of the cloud above the gravel pool showed by far the strongest combustion loads. Repeated spills in gravel beds might generate highly reactive condensed phase mixtures.

These results show that the use of gravel as ground material for filling stations should be reconsidered.

3.3.1.5 Condensed phase ignition

The condensed phase ignition experiments have been cancelled. However, HSL provided a thorough report (D4.8) covering experiments on the interaction between a LH_2 pool and water sprays, an analysis of solid-phase formation in LH_2 releases and post-ignition behaviour of solid-phase materials based on previous experimental work.

The tests performed showed that contact between water and LH_2 do not necessarily cause a Rapid Phase Transition (RPT) and gave reassurance that sprinklers and water jets could be used as mitigation measures to control the flow or accumulation of LH_2. However, the rate of vaporisation is enhanced and if the cloud ignited it could lead to a larger fireball.

3.3.2 Consequence assessment: analytical and numerical approach

More details about the analytical and numerical results and approaches can be found hereafter in the appendixes, in D4.2 “Computational investigation of ignition phenomena related to cryogenic hydrogen” and D6.5 “Detailed description of novel engineering tools for LH_2 safety”.

3.3.2.1 Ignition energy for H_2-air mixtures

UU developed an analytical tool to calculate the Minimum ignition energy (MIE) in hydrogen-air quiescent mixtures at ambient and cryogenic temperature. The analytical tool was validated against experiments for ambient temperature mixtures with hydrogen concentration in the air between 9 and 70%. The validation range was expanded to cryogenic mixtures with hydrogen concentration within the range 10-30% by comparison with experimental data from INERIS tests with the temperature of 173 K. The model is described in detail in Appendix 3.1.

- The developed analytical tool can be used to assess the potential of cryogenic hydrogen-air mixtures to ignite depending on its initial temperature and composition.

- A decrease of temperature of the hydrogen-air mixture leads to an increase of MIE for the same hydrogen concentration in air, confirming experimental observations.

Thus, the same safety measures as for ambient hydrogen-air mixtures may be employed.

3.3.2.2 Electrostatic charge generated in H_2 jets

KIT/PS investigated the electrostatic field built-up in warm (ambient temperature) and cold (approx. 80 K) jets and plumes using the DISCHA experimental setup and the cryovessel, both described in section 4.2.1.1.

In both configurations, strong electrostatic fields were observed. The measurements with the DISCHA setup showed that the electrostatic fields are stronger with increasing initial pressure and increasing nozzle diameter and a strong influence on ambient conditions was also observed. Especially the initial temperature plays an important role since much stronger fields (~100 larger) were measured in cold tests than in ambient temperature tests.

This observation, together with the fact that strong fields were only measured during the first 1 s of an experiment, leads to the assumption that the field generation might be connected with ice crystals that form at the cold nozzle prior to the release. When the release valve is opened these crystals are blown away and might generate the electric field by friction and rupture of the crystals.

3.3.2.3 CFD approach

- UU performed a CFD study to investigate numerically the condensation of oxygen over an evaporating LH_2 pool and its potential to cause highly energetic events after ignition. The study includes the assessment of the effect of wind parameters on the condensation of oxygen.
  - CFD modelling can be used to investigate the formation of cryogenic mixtures of H_2 and condensed O_2, which can potentially lead to highly energetic events in the case of ignition.
  - Simulation results showed that wind parameters affect the potential oxygen condensation. Wind direction tilted by 45 degrees towards the ground was found to lead to a potentially more dangerous scenario compared to the wind direction parallel to the ground.
  - The CFD tool can be used to determine a LH_2 pool size limit that would lead to hazardous conditions of condensed O_2/H_2 mixtures.

- UU developed a CFD model capable of reproducing the MIE by spark ignition of hydrogen-air mixtures. The CFD approach is based on a pressure-based implicit solver, a finite rate model for combustion with detailed chemical mechanisms and discrete ordinates for radiation. The CFD model has been validated against experiments with ambient temperature mixtures (from literature) and for cryogenic temperature mixtures against tests performed by INERIS within PRESLHY.

  - CFD modelling can be used to determine MIE of hydrogen air-mixture with H_2=10-60% by vol in air and temperature from 123 to 300 K.

- CFD modelling can give guidance on the effect of a mixture temperature on combustion properties.
- CFD simulations showed that the decrease of temperature of the hydrogen-air mixture leads to an increase of MIE for the same hydrogen concentration in air, confirming observations from experiments and analytical modelling.

- UU performed a CFD study assessing the effects of hydrogen temperature on the limit pressure leading to spontaneous ignition in a T-shaped channel with insertion of a burst disk. The CFD code used is ANSYS Fluent with a density-based explicit solver, a LES approach for turbulence, a finite rate model for combustion with a detailed chemical mechanism. The model has been previously validated against ambient temperature releases. The main findings of the CFD study relevant for guidelines are the following:

  - LES CFD approach can be used to simulate the spontaneous ignition phenomena in a T-shaped channel.
  - CFD modelling can be applied to determine the limit storage pressure leading to spontaneous ignition of a hydrogen release at cryogenic temperature in a T-shaped channel.
  - For ambient temperature hydrogen (300 K), a pressure of 2.9 MPa is required to obtain spontaneous ignition and likely transition into a jet fire outside the T-shaped channel. Pressure in the range 2.6-2.8 MPa can trigger ignition, but later result into self-extinction. A pressure of 2.43 MPa does not trigger ignition.
  - For cryogenic hydrogen (80 K), a pressure approximately 4 times larger than for ambient temperature hydrogen is required to trigger ignition and sustain combustion outside the T-shaped channel that could likely lead to a hydrogen jet fire. The pressure limit resulted to be 9.4 MPa. For pressure equal or below 8.75 MPa, there may be ignition in the T-shaped channel that then self-extinguishes.
  - The limit storage pressure leading to spontaneous ignition is strictly dependent on the geometry and characteristics of the release tube/system, e.g. presence of rupture disk, etc. Considerations above are valid for a T-shaped channel with insertion of a rupture disk.

3.3.3 Summary

Experiments:

The issues addressed in the experimental part of WP4 were the characterization of the fundamental ignition parameters of cryogenic hydrogen (MIE), the study of electrostatic ignition in cold jet and plume and ignition above a pool. Condensed phase ignition experiments were cancelled and replaced by experiments on RPT induced by sprinklers and water jets. The main observations are:

- There is a slight increase in MIE for cryogenic hydrogen in comparison with ambient temperature for the same hydrogen concentration in air. Consequently, the same safety measures as for ambient hydrogen-air mixtures may be employed.
- In small pressurized cryo jet experiments (with cold H_2 and LH_2), strong electrostatic fields were measured but no spontaneous ignition was recorded.
- In large-scale cold cloud experiments, the flow of LH_2 in pipes causes electrostatic charges. These findings could be used for either designing LH_2 pipework so that the development of two-phase flows are limited or ensuring that the pipework contains no electrically isolated sections.

- No spontaneous ignition was noted above the pool. The observed combustion behaviour of pools above concrete, water and sand is similar. However, the ignition of the cloud above the gravel pool showed by far the strongest combustion loads. These results show that the use of gravel as ground material for filling stations should be reconsidered.

- The tests performed did not generate Rapid Phase Transition (RPT) and gave reassurance that sprinklers and water jets could be used as mitigation measures to control the flow or accumulation of LH_2. However, the rate of vaporisation is enhanced and if the cloud ignited it could lead to a larger fireball.

Analytical tools:

- The analytical model in Appendix 3.1 can be used to assess the potential of cryogenic hydrogen-air mixtures to ignite.

Numerical tools:

- CFD modelling can be used to investigate the potential of LH_2 evaporating pools to form mixtures of cryogenic hydrogen and condensed oxygen for different wind conditions.
- CFD modelling can be used to accurately predict MIE by spark ignition for hydrogen-air mixtures and give guidance on the effect of a mixture temperature and hydrogen concentration on combustion parameters.

- CFD modelling can be applied to determine the limit storage pressure leading to spontaneous ignition of a hydrogen release at cryogenic temperature in a T-shaped channel.

3.4 Combustion of cryogenic hydrogen

3.4.1 Main outcomes from PRESLHY on combustion of cryogenic hydrogen

More details about the experiment setups can be found in the deliverable D2.6 "Refined Work Program". More details about the experimental results can be found in D5.3 "Experimental investigation of pre-mixed combustion phenomena with cryogenic hydrogen".

3.4.1.1 Jet fire

KIT performed jet fires using a similar facility as described in 4.2.1.1. The initial pressure varied from 5 to 200 bar, the temperature was ambient (280 K) or cryogenic (80 K), the nozzle diameter varied from 1 to 4 mm, the ignition position varied between 40 and 200 cm from the nozzle, the ignition duration was set at 1s and the ignition delay time from 20 to 900 ms.

These experiments allowed us to better understand transient jets and combustion processes. Flame flashback to nozzle was observed more often in cold experiments, especially for high pressure and large nozzle diameter. An iterative procedure is ongoing to identify most critical ignition time and location, and inventory based maps of worst effects (pressure & thermal) are to be extrapolated to large inventories.

3.4.1.2 Flame acceleration and DDT at cryogenic temperature

KIT and PS investigated the flame propagation regimes at cryogenic temperature in a cold tube of 5 m length and 5.4 cm in diameter. The temperatures used were ambient and 80 K, the hydrogen concentration varied from 6 to 75 Vol%, the blockage ratio used were 0, 30 and 60%, the initial pressure was constant at 1 bar. The objective was to evaluate the critical conditions for flame acceleration and detonation transition for hydrogen-air mixtures at cryogenic temperatures, possibly in the presence of condensed oxygen and nitrogen. This work is required for safety analysis and evaluation of the strongest possible combustion pressure and safety distances for LH_2 explosions.

Preliminary results concluded that an increase in critical and effective expansion ratios determine flame acceleration in cryogenic mixtures. The run-up distance for detonation transition was reduced in cryogenic mixtures due to density effects. The influence of blockage ratio on cold mixtures DDT is less pronounced.

3.4.1.3 Flame propagation over a spill

KIT observed the flame propagation over a spill. They used a semi-confined channel (300x60x40 mm) with an open ground face and LN_2-cooled ceiling. Pre-cooled H_2 from a pressurized reservoir was injected from the top into the channel to generate reproducible H_2 concentration gradients in the channel. The H_2 concentration profiles were measured in 3 positions in the channel in unignited distribution experiments. Immediately thereafter ignition experiments were done under the same initial conditions. The initial temperature

of the gas mixture was ambient or 80 K, the blockage ratio was 0, 30 or 60%, and the initial H_2 concentration was varied. Analysis of the data is on-going.

3.4.1.4 Flame propagation in obstructed /confined cold cloud

HSL carried out 23 trials where cryogenic hydrogen was released into a steel congestion frame, to examine the effect of different levels of congestion upon the ignition behaviour of a cryogenic hydrogen plume.

By comparing the results with those from a previous set of experiments in which LH_2 was released and ignited in the free field, it is clear that higher levels of volumetric congestion increase the measured overpressures in releases with the same initial conditions. The results also show that an increasing hydrogen inventory, through either an increased release pressure or larger nozzle, can result in a larger event upon ignition. However, the mixing of the jet also plays a part; some releases through the largest release orifice diameter showed lower overpressures potentially due to the hydrogen cloud being too rich.

Notwithstanding the variability introduced by the wind, the results suggest the following as a reasonable basis for risk assessment for some releases during tanker operations:

- Location with a low level of congestion: for the low level of congestion (volume blockage ratio <1.5%, area blockage <1m²/m^3, congestion length scale 25-50mm), there is little risk of uncontrolled flame acceleration. An assumption of TNO level 5 would be appropriately conservative, to be applied only to the portion of the cloud within the congested area. As a rule of thumb, if the entire cloud could be in the congested area, the explosive energy release for 1 bar tanker pressure would be approximately 20 MJ and for 5 bar pressure 50 MJ.
- Location with a high level of congestion: where there is a densely congested area (volume blockage ratio >4%, congestion length scale 25-50mm) with a volume of more than about 15 m^3 then it would be appropriate to assume that a high-level explosion or DDT could occur. It would be reasonable to assume that such an explosion could involve all of the cloud. As a rule of thumb, explosive energy release for 1 bar tanker pressure would be approximately 20 MJ and for 5 bar pressure 50 MJ.
- Unfortunately, the work could not define the boundary beyond which severe explosions happen with greater precision than this. Depending on the sensitivity of potential targets, it might be appropriate to assume that a severe explosion could occur for congested volumes of limited size or of intermediate levels of congestion. The reader should be aware that the assumptions made here are valid for this particular geometry. The size of the congestion region may also have an effect on the pressure and flame speed generated hence these assumptions may not apply to all cases.

The reader should be aware that the assumptions made here are valid for this particular geometry. The size of the congestion region may also have an effect on the pressure and flame speed generated hence these assumptions may not apply to all cases.

3.4.2 Consequence assessment: analytical and numerical approach

More details about the analytical and numerical results and approaches can be found hereafter in the appendixes, in D5.2 "Computational investigation of combustion phenomena with cryogenic hydrogen" and D6.5 "Detailed description of novel engineering tools for LH_2 safety".

3.4.2.1 Laminar burning velocity and expansion ratios for H_2-air mixtures

INERIS developed an analytical tool to estimate the influence of temperature on the laminar burning velocity of the flame and on the expansion ratio of the combustion for hydrogen-air mixtures at various fuel-air ratios at atmospheric pressure. The range of variations is intended to represent those potentially occurring during leakage of liquid hydrogen. The method includes graphs and correlations. More details can be found in Appendix 4.5.

3.4.2.2 Flame length correlation and hazard distance for jet fires

UU tested the dimensionless correlation for hydrogen jet flames calculating the flame length knowing the storage conditions for cryogenic ignited releases. The dimensionless correlation can be used for jet fires with pressure in the range 10 to 900 bar at 187 to 300 K (Molkov and Saffers, 2013) and temperatures down to 46 K in the range of 2 to 6 bara (Cirrone *et al.*, 2019).

The tool can be used to determine the hydrogen jet flame dimensions and associated hazard distances.

3.4.2.3 Thermal load from jet fires

UU developed a predictive tool to estimate the thermal radiation and thermal dose in the surroundings of momentum-dominated jet fires. The model is valid for jet fires with pressure from 2 to 900 bars and temperatures from 48 to 315 K.

This tool can be used to determine hazard distances based on thermal radiation harm criteria.

3.4.2.4 Pressure load from delayed ignition of turbulent jets

UU developed a semi-empirical correlation to estimate the maximum pressure load that could be expected from the delayed ignition of hydrogen turbulent jets, including cryogenic releases. The correlation is described in detail in Appendix 4.3.

- The engineering tool can be applied to hydrogen jets with storage pressure 0.5-65 MPa, storage temperature 80-300 K and release diameter 0.5-52.5 mm. The maximum validation distance of the target from the release source is 50 m.
- The study showed that maximum overpressure generated by delayed ignition is proportional to the square root of the ratio of the storage pressure to ambient pressure

and the square of the ratio of release diameter to the distance between the centre of the fast burning mixture in the jet (25-35% by volume) and the target location.

– The engineering tool can be used to determine conservative hazard distances for given storage conditions based on pressure load harm criteria for people and structure.

3.4.2.5 Flame acceleration and DDT for cryogenic H_2-air mixtures

KIT/PS developed a model dedicated to calculating critical hydrogen concentrations for effective flame acceleration and detonation onset for hydrogen-air combustion at cryogenic temperatures, for elongated channel or tube geometry with or without obstructions. Evaluation of Flame Acceleration (FA) and Detonation-to-Deflagration Transition (DDT) conditions at cryogenic temperatures depends on three major parameters:

- The geometry of the system:
  - Confinement degree (only confined is considered).
  - The geometry of the channel (smooth, rough, congested/blocked).
  - Scale (characteristic size – cross-section, length of the channel, length of the cloud of hydrogen-air mixture).
- Mixture characterization:
  - Mixture uniformity (only uniform is considered).
  - Initial pressure and temperature.
  - Mixture reactivity (laminar flame velocity, expansion ratio, speed of sound, detonation velocity, detonation pressure, detonation cell size.
- History and dynamics of the combustion process (run-up-distance, runway distance to flame acceleration and DDT).

The method is based on new experimental data on critical expansion ratio and detonation cell sizes in the temperature range 90-130 K, described here.

The tool can be used to evaluate the maximum combustion pressure resulting from a predicted flame propagation regime.

3.4.2.6 Fireball size after LH2 spill combustion

Correlation by Makarov *et al.* (2021) can be used to determine a fireball size after liquid hydrogen spill combustion. A detailed description is given in Appendix 4.5.

3.4.2.7 CFD modelling activities

- UU developed a CFD model to predict thermal hazards from cryogenic hydrogen jet fires validated against the experiments performed by SNL (Panda and Hecht, 2017) and KIT tests from the ICEFUEL project (Breitung *et al.*, 2009). The CFD model used is ANSYS Fluent with a steady-state pressure-based solver, a RANS approach for turbulence, an EDC model for combustion with detailed chemical mechanism and DO for radiation modelling. The range of application of the model is 48 to 80 K in temperature, 2 to 20 bar in pressure and nozzle diameter from 1.25 to 4 mm.

- The developed CFD approach can be used to accurately reproduce thermal radiation from hydrogen jet fires as proven by validation against experiments.
- Simulations showed that buoyancy of combustion products has a positive effect on the reduction of the "no harm" distance by temperature from $x=3.5L_f$ for vertical jet fires to $x=2.2L_f$ for horizontal jet fires, where L_f is the jet fire flame length.
- Simulations showed that thermal radiation leads to longer "no-harm" distances ($x=3.2L_f$) in the direction of the jet compared to the hazard distance defined by temperature.
- Thermal dose proved to be a useful parameter to define hazard distances for emergency personnel.
- The CFD approach can be used to assess hazard distances for horizontal jet fires with inclusion of the buoyancy effect on high temperature combustion products and hot currents.

- Releases of hydrogen in a confined space with limited ventilation can produce transient pressure dynamics with a distinctive peak exceeding the steady state pressure. This is defined as the pressure peaking phenomenon (PPP), and is particularly pronounced for hydrogen as characterised by the lowest density. The magnitude of the peak pressure depends mainly on hydrogen release rate, ventilation rate and enclosure volume.
  - Ignited releases lead to a more pronounced PPP compared to unignited releases.
  - CFD approach can be used to assess the effect of cryogenic storage temperature on PPP from ignited hydrogen releases.
  - Simulations showed that the decrease of storage temperature for a same nozzle diameter and storage pressure causes an increase in hydrogen mass flow rate, and, thus, higher peak overpressure. For a storage pressure equal to 11.78 MPa, a decrease of storage temperature from 277 K to 100 K can cause an increase of peak overpressure by over a factor of 2.
  - The effect of storage temperature decrease on PPP should be considered in the design of TPRD size for cryo-compressed hydrogen storages.

3.4.3 Summary

Experiments:

The issues addressed in the experimental part of WP5 were the characterization of jet fires, flame acceleration and deflagration to detonation transition as well as the flame propagation in an obstructed/confined area. The main observations are:

- The jet fire experiments allowed a better understanding of transient jets and combustion processes. Flame flashback to nozzle was observed more often in cold experiments, especially for high pressure and large nozzle diameter.

- Results concluded that an increase in critical and effective expansion ratios determine flame acceleration in cryogenic mixtures. The run-up distance for detonation transition was reduced in cryogenic mixtures due to density effects. The influence of blockage ratio on cold mixtures DDT is less pronounced.
- The following results are considered a reasonable basis for risk assessment of a release in an obstructed area, for a congested region of similar size as the one used by HSE:
  - For low levels of congestion, the risk of uncontrollable flame acceleration is low. An assumption of TNO level 5 would be conservative to be applied to the cloud within the congested area.
  - For high levels of congestion, it is appropriate to assume that a high-level explosion or DDT could occur.
  - Some additional experimental work is required to determine with more precision the boundary beyond which severe explosions happen. It might be appropriate to assume that a severe explosion could occur for intermediate levels of congestion.

Analytical tools:

- The analytical tool in Appendix 4.5 can be used to estimate the influence of temperature on the laminar burning velocity of the flame and on the expansion ratio of the combustion for hydrogen-air mixtures at various fuel-air ratios at atmospheric pressure.

- The dimensionless correlation for hydrogen jet flames by Molkov and Saffers (2013) can be used to estimate a cryogenic gaseous hydrogen jet fire flame length and associated hazard distances, Appendix 4.1.

- The engineering tools in appendix 4.2 and 4.3 can be used to estimate respectively the thermal radiative heat flux and thermal dose in the surroundings of a cryogenic hydrogen jet fire, and the maximum overpressure that can be expected from delayed ignition of a hydrogen jet fire for given storage conditions and nozzle diameter, and their associated hazard distances.

- A model described in Appendix 5.1 can be used to calculate critical hydrogen concentrations for effective flame acceleration and detonation onset for hydrogen-air combustion at cryogenic temperatures for elongated channel or tube geometry with or without obstructions. The tool can be used to evaluate the maximum combustion pressure resulting from a predicted flame propagation regime.

- The correlation described in Appendix 4.6 can be used to determine a fireball size after liquid hydrogen spill combustion.

Numerical tools

- The CFD approach can be used to assess hazard distances for horizontal jet fires with inclusion of the buoyancy effect on high temperature combustion products and hot currents.

- The CFD approach can be used to assess the effect of cryogenic storage temperature on PPP from ignited hydrogen releases.

4 Conclusions

This report provides a summary of the main research results from experimental, analytical and numerical work that has been performed during the pre-normative research project PRESLHY in order to understand poorly understood phenomena related to LH_2 and develop the necessary tools for hydrogen safety.

The following recommendations were drawn from the experimental work:

- No rainout was observed and pools formed only for vertical releases. However, rainout can not be ruled out as a credible scenario for the moment.
- Pools could form on any of the substrates tested but the delay of formation is longer when the material has a high porosity. However, the ignition of the cloud above the gravel pool (highly porous) showed by far the strongest combustion loads in comparison with sand, concrete and water. These results show that the use of gravel as ground material for filling stations should be reconsidered.
- The ignition properties of hydrogen are affected very little by the temperature. The MIE of cryogenic hydrogen is slightly higher than for ambient hydrogen and there is no change in hot surface temperature. Consequently, the same safety measures as for ambient hydrogen-air mixtures may be employed.
- In small and large-scale releases, strong electrostatic fields were observed but no spontaneous ignition occurred. In large-scale releases, the flow of LH_2 in pipes causes electrostatic charges so it is advised to design LH_2 pipework to limit the development of two-phase flows and ensure that the pipework contains no electrically isolated sections.
- The use of sprinklers and water jets on a pool of LH_2 did not generate any RPT so they can be employed as mitigation measures to control the flow or accumulation of LH_2. However, they enhance the vaporization rate that could lead to a larger fireball if the cloud is ignited.
- The run-up distance for detonation transition was reduced in cryogenic mixtures due to density effects but the influence of blockage ratio on cold mixtures DDT is less pronounced.
- For risk assessment of a release in an obstructed area:
    - For low levels of congestion, the risk of uncontrollable flame acceleration is low. An assumption of TNO level 5 would be conservative to be applied to the cloud within the congested area, depending on its size.
    - For high levels of congestion, it is appropriate to assume that a high-level explosion or DDT could occur.
    - It might be appropriate to assume that a severe explosion could occur for intermediate levels of congestion. However, some additional experimental work is required to determine with more precision the boundary beyond which severe explosions happen.

- As a rule of thumb, if the entire cloud could be in the congested area, the explosive energy release for 1 bar tanker pressure would be approximately 20MJ and for 5 bar pressure 50MJ.

For the design and consequences assessment, several calculation means have been developed during the project. Simple engineering tools, as well as numerical simulation tools, are presented in this report and the full details about their range of applicability and validation can be found in the appendixes of this report and in the deliverable D6.5 "Detailed description of novel engineering tools for LH_2 safety".

One relevant aspect of PRESLHY to the industry is the determination of hazard distances for liquid hydrogen installations. For this purpose, the following tools have been developed:

- The similarity law has been validated for cryogenic jets and can be used to determine the distance to LFL;
- A correlation for hydrogen jet flames can be used to estimate a cryogenic gaseous hydrogen jet fire flame length and associated hazard distances;
- An engineering tool for cryogenic hydrogen jet fire can be used to estimate the thermal radiative heat flux and thermal dose in the surroundings and associated hazard distances;
- An engineering tool for hydrogen jet fire can be used to estimate the maximum overpressure that can be expected from its delayed ignition and associated hazard distances;
- A correlation for spills can be used to determine a fireball size after liquid hydrogen spill combustion;
- A CFD approach can be used to assess hazard distances for horizontal jet fires with the inclusion of the buoyancy effect.

References

Breitung, W., Stern, G., Veser, A., Friedrich, A., Kutznetsov, M., Fast, G., Oechsler, B., Kotchourko, N., Travis, J.R., Xiao, J., Schwall M. (2009), *Final Report: Experimental and theoretical investigations of sonic hydrogen discharge and jet flames from small breaks*.

Chen, C. and Rodi, W. (1980), *Vertical Turbulent Buoyant Jets - a review of experimental data*, Pergamon Press, Oxford.

Cirrone D., Makarov D., Molkov, V. (2019), *Cryogenic hydrogen jets: calculation of hazard distances*. International Conference on Hydrogen Safety, 24th-26th September 2019, Adelaide, Australia.

Cirrone, D., Makarov, D., Kuznetsov, M., Friedrich, A., Molkov, V. (2021), *Effect of heat transfer through the release pipe on simulations of cryogenic hydrogen jet fires and hazard distances*, submitted to International Conference on Hydrogen Safety, Edinburgh, Scotland.

Coward, H.F. and Jones, G.W. (1952) Limits of flammability of gases and vapors. Bureau of Mines, US government printing office, Washington.

Friedrich, A., Veser, A. and Jordan, T. (2019) PRESLHY – D3.4 Summary of Experiment Series E3.1 (Discharge) Results.

Hecht, E.S. and Panda, P.P. (2019) Mixing and warming of cryogenic hydrogen releases. Int. J. of Hydrogen Energy 44: 8960-8970.

Makarov, D., Shentsov, V., Kuznetsov, M. and Molkov, V. (2021) *Hydrogen Tank Rupture in Fire in the Open Atmosphere: Hazard Distance Defined by Fireball*, Hydrogen, Vol. 2 No. 1, pp. 134–146.

Molkov, V.V. (2012) Fundamentals of hydrogen safety engineering, www.bookboon.com.

Molkov, V. and Saffers, J. B. (2013), Hydrogen Jet Flames, International Journal of Hydrogen Energy, vol. 38, no. 19, pp. 8141–8158.

Panda, P. P. and Hecht, E. S. (2017) *Ignition and Flame Characteristics of Cryogenic Hydrogen Releases*, International Journal of Hydrogen Energy 42 (1), 775–785.

Saffers, J. B. and Molkov, V. V. (2013), *Towards Hydrogen Safety Engineering for Reacting and non-Reacting Hydrogen Releases*, Journal of Loss Prevention in the Process Industries, vol. 26, no. 2, pp. 344–350.

Saffers, J.-B. and Molkov, V.V. (2014) Hydrogen Safety engineering framework and elementary design safety tools, Intl. J. of Hydrogen Energy 39: pp. 6268 – 6285.

Schefer, R.W., Houf, W.G., Williams, T.C., Bourne, B. and Colton, J. (2007), *Characterization of high-pressure, underexpanded hydrogen-jet flames*, International Journal of Hydrogen Energy, Vol. 32, pp. 2081–2093.

Schroder, V. and Holtappels, K. (2005) Explosion characteristics of hydrogen-air and hydrogen-oxygen mixtures at elevated pressures. Int. Conf. on Energy Materials.

Veser, A., Friedrich, A., Kuznetsov, M., Jordan, T. and Kotchourko, N. (2021) Hydrogen blowdown release experiments at different temperatures in the DISCHA facility. 9th Int. Conf. on Hydrogen Safety, 21-23 Sept. 2012, Edinburgh, UK.

Appendices

Appendix 1. Harm criteria

- Oxygen depletion: hydrogen concentration between 9% and 28% by volume would affect evacuation and would be life threatening at above 42% (HySafe, 2007).
- Direct contact with the flame:
  - British Standards (BSI, 2004) recommends 115°C as the threshold for pain from an elevated air temperature for exposure exceeding 5 minutes.
  - DNV (2001) proposed the following classification of temperature effects on occupants:
    - Below 70°C, no fatal issue in a closed space except uncomfortable situation;
    - Between 70°C and 150°C, the impact is dominated by difficulties to breath;
    - Above 150°C, skin burns occur in less than 5 minutes. This is considered a threshold temperature for escape;
    - At 309°C, third degree burns for a 20s ("death") limit.
  - Time to incapacitation in minutes as a function of air temperature (°C) can be estimated by the following equations recommended by DNV (2001) and BSI (1997) respectively:

$$t_{incap} = 5.33 * 10^8 * T_{air}^{-3.66} \quad \text{(Eq. A1.1)}$$

$$t_{incap} = 5 * 10^7 * T_{air}^{-3.4} \quad \text{(Eq. A1.2)}$$

  - For the acceptance threshold temperature of 115°C, Eqs. (A1.1) and (A1.2) provide incapacitation time of 5 minutes and 15 minutes of exposure respectively.
  - Bryan (1986) and DNV (2001) provide more details on physiological response of humans to air at elevated temperature (Table A1.1):

Table A1.1: Effect of air temperature on people (Bryan, 1986; DNV, 2001).

Temperature	Effect on people
127°C	Difficult breathing
149°C	Mouth breathing difficult, temperature limit for escape
160°C	Rapid, unbearable pain with dry skin
182°C	Irreversible injuries in 30 seconds
203°C	Respiratory systems tolerance time less than four minutes with wet skin
309°C	Third degree burns for 20 seconds exposure, causes burns to larynx after a few minutes, escape improbable

  - Figure A1.1 illustrates time to incapacitation as a function of duration of exposure calculated using Eq. (A1.1) and (A1.2). Note that for the lower temperatures (the dash lines) the use of these equations is not relevant.

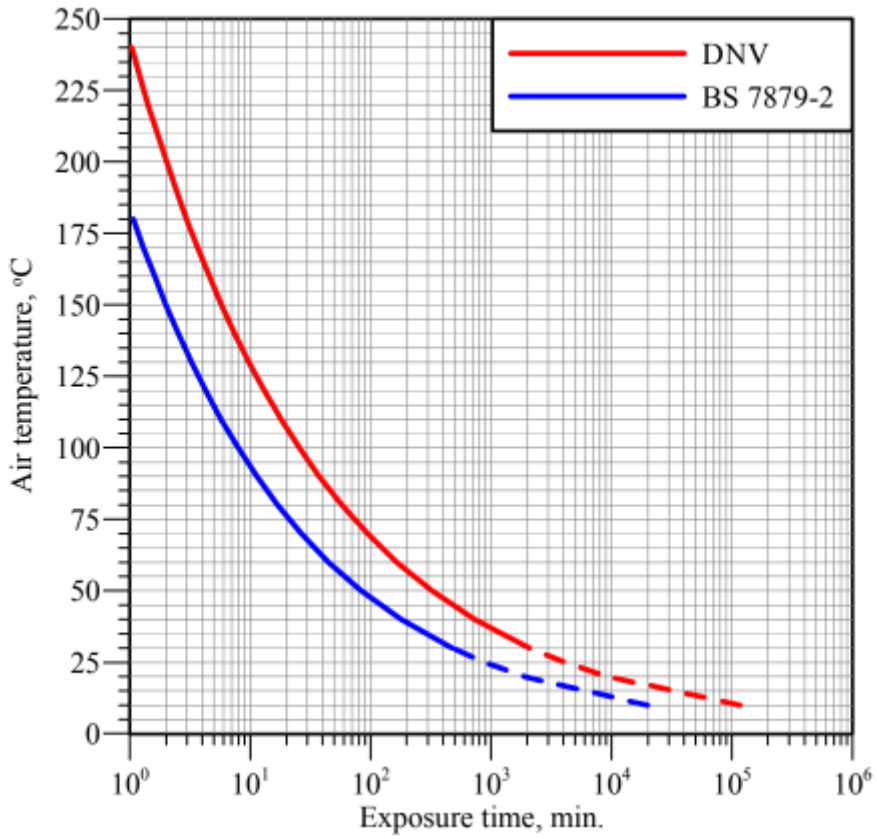

Figure A.1.1: Time to incapacitation as a function of duration of exposure calculated using BSI (1997) – red curve, and DNV (2001) – blue line - approaches (Saffers, 2010).

- Radiant heat flux:
  - 1.5 kW/m² radiant flux is considered safe for the members of public (Saffers, 2010).
  - 2.5 kW/m² radiant flux is considered the tolerable value for building occupants. Pain and first-degree burn will occur after 38 seconds exposure but do not prevent from evacuating (Saffers, 2010). According to BSI (2004), this level of intensity can be withstood for more than 5 minutes.
  - 5 kW/m² radiant flux can be considered a threshold of tolerability for emergency responders with protective clothing (Saffers, 2010). Raimundo and Figueirido (2009) set this value at 7kW/m² and Lees (1996) at 4.7 kW/m². Long exposure should be avoided.
  - The intensity of 6 kW/m² is tolerable for occupants when evacuating and is an important threshold value. This intensity is lethal in about 38 seconds and pain is reached in just 12 seconds (Saffers, 2010).
  - Table A1.2 has been compiled by Saffers (2010) based on Lees (1996), BSI (2004), Pasman (2006) and Raimundo and Figueirido (2009).

Table A1.2: Effect of radiant heat flux on people (Saffers, 2010)

Radiant heat flux (kW/m²)	**Effects on people**
1.5	Intensity safe for stationary personnel and members of the public
2.5	Intensity tolerable over 5 min.; severe pain above this threshold
3	Intensity tolerable in infrequent emergency situations for 30 min.
5	Intensity tolerable for performing emergency operations
6	Intensity tolerable to escaping emergency personnel
9.5	Second degree burn after 20 seconds
12.5 to 15	First degree burn after 10 seconds, 1% fatality in 1 minute
25	Significant injury in 10 seconds, 100% fatality in 1 minute
35 to 37.5	1% fatality in 10 seconds

- For buildings and structures, the light damage threshold can be set at 5kW/m² as it is the intensity at which the windows break, and the moderate damage threshold at 10 kW/m² (Saffers, 2010).
- Table A1.3 summarizes the effects of intensity of radiant heat flux on structures and environment (Lees, 1996):

Table A1.3: Effects of radiant heat flux to structures and environment (Lees, 1996).

Radiant heat flux (kW/m²)	**Effects on structure and environment**
5	Intensity for significant windows breakage
8-12	Intensity for domino effects
10	Heating of structures; increase of temperature and pressure in liquid/gas storages
10 -12	Intensity for vegetation to ignite
16	Intensity for failure of structures in prolonged exposure (except concrete)
20	Intensity concrete structures can withstand for several hours
30	Intensity for non-piloted ignition of wood occurs
38	Intensity for damages caused to process equipment and storage tanks
100	Steel weakening
200	Intensity for concrete structures to fail in several dozen of minutes

- Thermal dose (LaChance *et al.*, 2011):
  - 80-130 $(kW/m^2)^{4/3}s$ is the threshold range for first-degree burns for exposure to infrared radiation. 260-440 $(kW/m^2)^{4/3}s$ range is indicated for exposure to ultraviolet radiation.
  - 240-730 $(kW/m^2)^{4/3}s$ is the threshold range for second-degree burns for exposure to infrared radiation. 670-1100 $(kW/m^2)^{4/3}s$ range is indicated for second-degree burns from exposure to ultraviolet radiation.
  - 870-2640 $(kW/m^2)^{4/3}s$ is the threshold range for third-degree burns for exposure to infrared radiation. 220-3100 $(kW/m^2)^{4/3}s$ range is indicated for third-degree burns from exposure to ultraviolet radiation.
- Overpressure:
  - Overpressure can affect life safety through both direct (damage to persons from the overpressure itself) and indirect (damage produced by body displacement due to drag force, structural collapse and flying debris, such as glass shards from broken windows, etc.) effects.
  - Structures are more prone to be impacted by a blast wave than people are. Indirect damage to the occupant indoors (e.g. from the glass shards) can require more stringent safety threshold than direct damage. NATO field manual (NATO, 1993) states that the indirect blast injuries are so predominant that people exposed only to direct blast injuries make up a small part of the patient workload. Windowpanes are particularly easy to break at very low pressures. Fragments can become missiles and impact people.
  - Saffers (2010) proposed 1 kPa as the tolerable value of overpressure for the public indoors. It corresponds to the breakage of 5% of windows as described in Table A1.6. 3 kPa is the threshold of injuries by glass fragments, while 10 kPa is the threshold of serious injuries by glass fragments.
  - The maximum value of overpressure for occupants indoors can be taken as 10 kPa, above which there are serious injuries and some fatalities (Saffers, 2010). For comparison, outdoors, at 8 kPa, there are no serious injuries from direct impact of the blast wave and 21 kPa is the threshold of survivability. Lees (1996) cites the Department of the Army (1969) in defining the range 15-20 kPa as the threshold for serious wound outdoors.
  - The peak overpressure of 34 kPa is the threshold for eardrum rupture. This provokes deafness, tinnitus and vertigo (Finkel, 2006), which would significantly impact evacuation.
  - Table A1.4 compiled by Saffers (2010) provides peak values of overpressure and associated level of injury to people indoors and outdoors based on data by Hansen *et al.* (2007), APPEA (1998), Jeffries *et al.*, (1997) and HSE (2006).

Table A1.4: Classification of level of direct and indirect injury to people depending on overpressure (Saffers, 2010), from Hansen et al. (2007), APPEA (1998), Jeffries et al. (1997) and HSE (2006).

Overpressure (kPa)	**Direct effects on people**
8	No serious injury to people outdoors
10	Serious injuries to people indoors, few fatalities
21	Threshold for survivability 20% probability of fatality to people indoors 0% probability of fatality outdoors
30	Many fatalities indoors (domestic properties)
34	Eardrum rupture
35	50% probability of fatality indoors 15% probability of fatality outdoors
54	Fatal head injury
62	Severe lung damage
70	100% probability of fatality indoors or in unprotected structures
82	Severe injury or death
	Indirect effects on people
3	Injuries by glass fragments to people indoors
6.9 – 13.8	Threshold of skin lacerations by missiles
10.3 -20	People knocked down by pressure wave
13.8	Possible fatality by being projected against obstacles
27.6 – 34.5	50% probability of fatality from missile wounds
48.3 -68.9	100% probability of fatality from missile wounds

- For the people outdoors, Barry (2003) provides the following estimate of peak values of overpressure and associated level of injury in Table A1.5.

Table A1.5: Overpressure peak values and injury levels (Barry, 2003).

Overpressure (kPa)	**Injury level**
8	No serious injury to people
6.9 – 13.8	Threshold of skin lacerations by missiles
10.3 – 20	People are knocked down by pressure wave
13.8	Possible fatality by being projected against obstacles
34	Eardrum rupture
35	15% probability of fatality
54	Fatal head injury
62	Severe lung damage
83	Severe injury or death

- Figure A1.2 shows the plots of the probit functions for eardrum rupture and death by lung haemorrhage cited in Lees (1996) and for human fatality cited by HSE (2006).

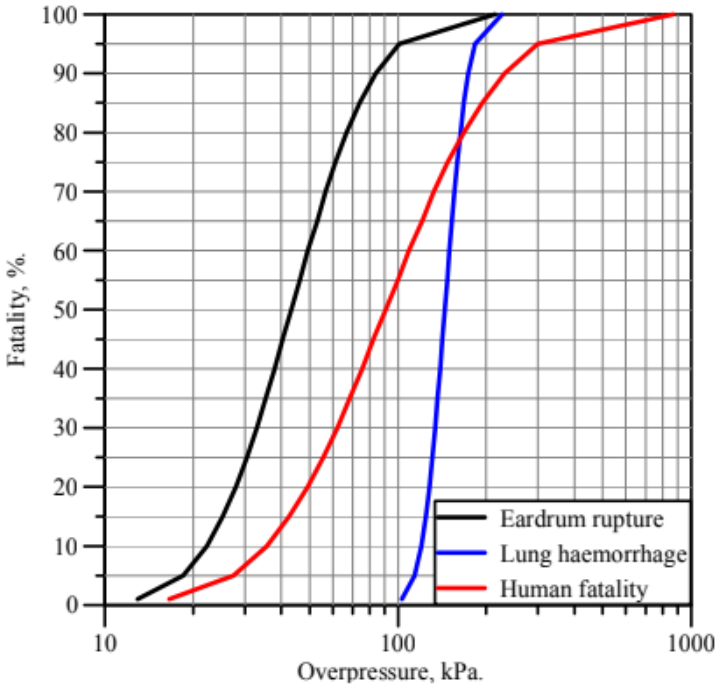

Figure A1.2: Probability of fatality, death by lung haemorrhage and eardrum rupture as a function of peak overpressure (Saffers, 2010).

- Table A1.6 compiled from Scilly and High (1986) and Lees (1996) summarizes the effect of overpressure on structures.

Table A1.6: Structural response to peak overpressure Scilly and High (1986), Lees (1996).

Elements	**Overpressure (kPa)**	**Failure**
Window pane	0.7 - 1	5% broken
	1.4 - 3	50% broken
	3 – 6	90% broken
Building	1.4 -3	Inhabitable after repair damage to ceilings, window and tiling
	3 – 6	Limited minor structural damage. Partitions and joinery was wrenched from fixings. Damage to house ceilings; 10% window glass broken
	6 – 9	Doors and window frame broken in
	9	Steel frame of clad building slightly distorted
	14 – 28	Uninhabitable; partial or total collapse of roof, partial demolition of one or two external walls, severe damage to load-bearing partitions
		Concrete or cinder block walls, not reinforced, shattered
	30	Destruction of all buildings that were not designed to withstand explosions
	35 – 80	50 to 75% external brickwork destroyed or rendered unsafe
	80 – 126	Almost complete demolition
	50 - 100	Displacement of cylindrical storage, failure of pipes

- A pressure peak for domino effects may also be defined at a value of 20 kPa (Guide to the effects of accidents, 2004) and used as threshold when applying the Control of Major Accident Hazards (COMAH) Regulations (Saffers, 2010).
- The damages listed in the table 6 can be classified and summarized as in Table A1.7 (Stephens, 1970):

Table A1.7: Classification of damages to structures depending on overpressures (Stephen, 1970).

Overpressure (kPa)	Damage level
< 3.5	Light damage
> 17	Moderate damage
>35	Severe damage
>83	Total destruction

- Blast waves effects depend on both peak overpressure and impulse. The following threshold values has been proposed (Saffers, 2010):
  - The sensitive area threshold would be set at 20 kPa.
  - The light damages threshold could be set at 3 kPa with an impulse greater than 100 Pa*s. At this overpressure, the infrastructure is inhabitable after repair damage to ceilings, windows and tiling. For overpressure above 3 kPa but with an impulse lower than 100 Pa*s, the threshold is shown in Figure A1.3.
  - The moderate damages threshold could be set at 15 kPa with an impulse greater than 300 Pa*s. For overpressure between 15 kPa and 35 kPa but with an impulse lower than 300 Pa*s refer to Figure A1.3.
  - The collapse threshold is set at 35 kPa with an impulse greater than 500 Pa*s. For overpressure higher than 35 kPa but with an impulse lower than 500 Pa*s, refer to Figure A1.3.

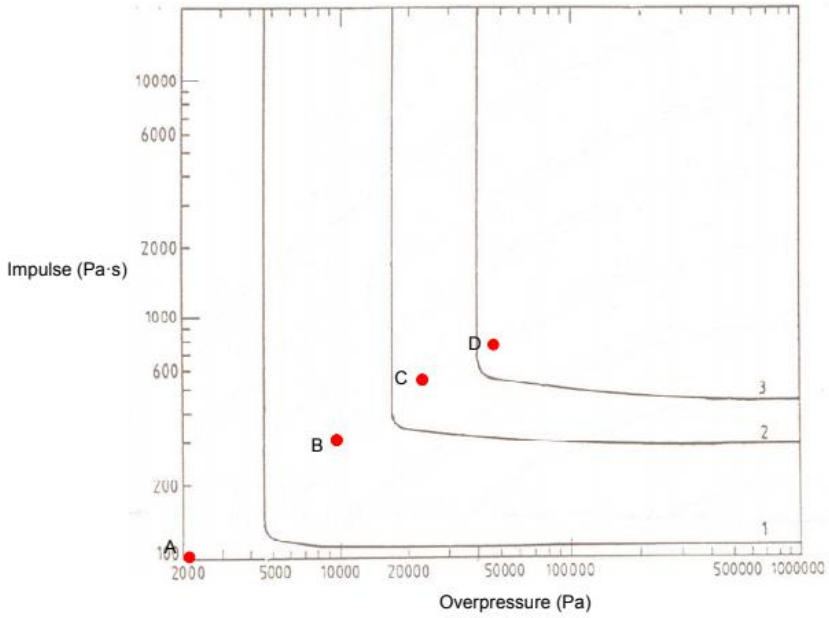

Figure A1.3: Overpressure-impulse diagram of a high explosive charge on the ground, producing a gradual level of damage to houses: Level 1 light, level 2 structural damage and level 3 collapse (Mercx et al., 1991). Markers A, B, C and D corresponds to damage level thresholds described by Baker et al. (1983) and Jarrett (1968) (see Table A.1.8).

Table A.1.8: Classification of damages to structures, depending on overpressure and impulse (Baker et al. (1983), and Jarrett (1968) via Saffers, 2010)

Peak overpressure (kPa)	**Impulse (kPa*s)**	**Damage description**	**Representation in figure A1.3**
3.6	0.10	Border of minor structural damages	A
14.6	0.30	Threshold for moderate structural damages: some load bearing element fail	B
34.5	0.52	Threshold for partial destructions: 50% to 75% of walls destroyed	C
70.1	0.77	Total destruction of buildings	D

- Cold burn from liquid hydrogen spill

Cryogenic liquids and the associated cold vapours have effects on the skin similar to a thermal burn. Brief exposures may not affect skin from the face or hands but can affect more delicate tissues such as the eyes. A prolonged exposure of the skin to cold environment or contact with cold surfaces can cause frostbite. Similarly, prolonged breathing of extremely cold air may damage the lungs. Unprotected skin can stick to metallic material cooled by cryogenic liquids, which will cause the skin to tear when pulled away. Non-metallic materials are also dangerous to touch at cryogenic temperatures.

Table A1.9: Exposure time to cold temperature before having frostbite on exposed skin (ACGIH, 2018). Even though not related to cryogenics, this table is a good guideline.

WIND CHILL TEMPERATURE INDEX
Frostbite Times are for Exposed Facial Skin

Air Temperature (°C)

Wind Speed (km/h)	5	0	-5	-10	-15	-20	-25	-30	-35	-40	-45	-50
5	4	-2	-7	-13	-19	-24	-30	-36	-41	-47	-53	-58
10	3	-3	-9	-15	-21	-27	-33	-39	-45	-51	-57	-63
15	2	-4	-11	-17	-23	-29	-35	-41	-48	-54	-60	-66
20	1	-5	-12	-18	-24	-30	-37	-43	-49	-56	-62	-68
25	1	-6	-12	-19	-25	-32	-38	-44	-51	-57	-64	-70
30	0	-6	-13	-20	-26	-33	-39	-46	-52	-59	-65	-72
35	0	-7	-14	-20	-27	-33	-40	-47	-53	-60	-66	-73
40	-1	-7	-14	-21	-27	-34	-41	-48	-54	-61	-68	-74
45	-1	-8	-15	-21	-28	-35	-42	-48	-55	-62	-69	-75
50	-1	-8	-15	-22	-29	-35	-42	-49	-56	-63	-69	-76
55	-2	-8	-15	-22	-29	-36	-43	-50	-57	-63	-70	-77
60	-2	-9	-16	-23	-30	-36	-43	-50	-57	-64	-71	-78
65	-2	-9	-16	-23	-30	-37	-44	-51	-58	-65	-72	-79
70	-2	-9	-16	-23	-30	-37	-44	-51	-58	-65	-72	-80
75	-3	-10	-17	-24	-31	-38	-45	-52	-59	-66	-73	-80
80	-3	-10	-17	-24	-31	-38	-45	-52	-60	-67	-74	-81

FROSTBITE GUIDE

Increasing risk of frostbite for most people in 10 to 30 minutes of exposure
High risk for most people in 5 to 10 minutes of exposure
High risk for most people in 2 to 5 minutes of exposure
High risk for most people in 2 minutes of exposure or less

References

ACGIH (2018) Threshold limit values (TLVS) and biological exposure indices (BEIS).

APPEA (1998) Australian petroleum production & exploration association limited (APPEA), Guidelines for fire and explosion management.

Baker, W.E., Cox, P.A., Kulosz, J.J., Strehlow, R.A. and Westine, P.S. (1983) Explosion hazards and evaluation, Fundamental studies in Engg. 5, Elsevier.

Barry, T.F. (2003) Fire exposure profile modelling: some threshold damage limit (TDL) data.

Bryan, J.L. (1986) Damageability of buildings, contents and personnel from exposure to fire, Fire safety Journal, 11: 15-31.

BSI (1997) British standard 7899-2:1997. Code of practice for assessment of hazard to life and health from fire. Guidance on methods for the quantification of hazards to life and health and estimation of time to incapacitation and death in fires. British Standards Institution.

BSI (2004) British standard Published Document PD 7974-6:2004. The application of fire safety engineering principles to fire safety design of buildings. Human factors. Life safety strategies. Occupant evacuation, behaviour and condition (Sub-system 6). British Standards Institute.

Department of the Army (1969) Nuclear Handbook for Medical Service Personnel. Technical manual TM8-215.

DNV Technica (2001) Human resistance against thermal effects, explosion effects, toxic effects and obscuration of vision.

Finkel, M.F. (2006) The neurological consequences of explosives, Journal of the Neurological Sciences, 249: 63-67.

Hansen, O., Middha, P., Marangon, A., Carcassi, M., Ham, K., Versloot, N. (2007) Description of a gaseous hydrogen refuelling station – Benchmark base case (BBC) for HyQRA IP 3.2. HyQRA BBC Station description (V1) 1-14.

HSE (2006) Health and Safety Executive. Indicative human vulnerability to the hazardous agents present offshore for application in risk assessment of major accidents. SPC/Tech/OSD/30.

HySafe (2007) Biannual report on hydrogen safety, HySafe, June 2007.

Jarrett, D.E. (1968) Derivation of British Explosive Safety Distances, Annals of the New York Academy of Sciences, 152: 18-35.

Jeffries, R.M., Hunt, S.J., Gould, L. (1997) Derivation of fatality probability function for occupants buildings subject to blast loads.

LaChance, L., Tchouvelev, A., Engebo, A. (2011) Development of uniform harm criteria for use in quantitative risk analysis of the hydrogen infrastructures. International Journal of Hydrogen Energy 36, 2381-2388.

Lees, F.P. (1996) Loss Prevention in the Process Industries, 2nd Edition, Butterworth - Heinemann, Oxford, UK.

Mercx, W.P.M., Weerheijm, J., Verhagen, T.L.A. (1991) Some considerations on the damage criteria and safety distances for industrial explosions, 11th Symposium on New Directions in Process Safety – Hazards, 124: 255-275.

NATO (1993) NATO, Field manual, health service support in a nuclear, biological and chemical environment. Fm 8-10-7 Headquarters, Department of the army, Washington, D.C.

Pasman, H.J. (2006) The challenge of risk control in a hydrogen based economy. Proceedings of the 1st European Summer School on Hydrogen Safety.

Raimundo, A.M. and Figueiredo, A.R. (2009) Personal protective clothing and safety of firefighters near a high intensity fire front. Fire Safety Journal 44(4): 514-521.

Saffers, J.-B. (2010) Principles of hydrogen safety engineering, PhD Thesis, University of Ulster, Belfast, UK.

Scilly, N.F. and High, W.G. (1986) The blast effects of explosions. Proceedings of the 5th International Symposium on Loss Prevention and Safety Promotion in the Process Industries 39-1-39-15.

Stephens, M.M. (1970) Minimising damage to refineries from nuclear attack, natural and other disasters. Office of Oil and Gas, Department of Interior.

Appendix 2. Engineering tools for liquid and cryogenic hydrogen releases

Appendix 2 presents the engineering correlations and tools supporting the guidelines related to cryogenic releases that were developed and validated within PRESLHY project. Each section describes briefly the aim of the tool, the implementation procedure, the validation range and an example of application. The full description, including how the engineering correlations and tools were obtained and the validation process, is reported in detail in PRESLHY deliverable D6.5 "Detailed description of novel engineering correlations and tools for LH2 safety, version 2".

A2.1 Determination of a cryogenic gaseous release rate (UU)

At release pressures above 2 bar abs, an under-expanded jet is expected, as pressure at the nozzle exit is above atmospheric. The under-expanded jet theory by Molkov *et al.* (2009) can be employed to calculate the flow parameters and mass flow rate at the release nozzle. The approach employs the Abel-Noble Equation of State (EoS) to describe the non-ideal behaviour of the gas at low temperatures. Release conditions are calculated assuming choked flow at the nozzle, isentropic expansion and conservation of energy between the stagnation and release locations. The under-expanded jet theory employing Abel-Noble EOS was found to reproduce release rate accurately for experiments with release temperature down to 37 K and pressure in range 2-6 bar abs (Cirrone *et al.*, 2019). The engineering tool is available on the e-laboratory platform developed within Net-Tools (https://elab-prod.iket.kit.edu/).

The same under-expanded jet theory assumptions and conservation equations can be used along with NIST EoS, which is based on the explicit modelling of the Helmotz free energy and is widely suggested for cryogenic hydrogen applications. The entropy and enthalpy at the storage conditions, s_0 and $h_0$respectively, are determined from the stagnation temperature and pressure, given that the fluid is in single-phase conditions. The conditions at the nozzle are then iteratively calculated gradually decreasing temperature along the isentropic expansion transformation from the "storage" conditions $s(T,P)=s_0(T_0,P_0)$, until the equation of energy conservation between storage and exit nozzle is satisfied with a given tolerance:

$$h_n - h_0 + \frac{(u_n)^2}{2} = 0$$

Enthalpy, h_n, and speed of sound, u_n, at the exit nozzle can be determined by open-source databases implementing NIST EoS (see Bell *et al.*, 2014). For temperature down to 46 K and pressure up to 6 bar abs, the maximum variation in the mass flow rates calculated with NIST EoS and Abel-Noble EoS is 7%, indicating that the two EOSs can be used interchangeably without affecting significantly the resulting release rate.

Full details on the engineering tool implementation are given in PRESLHY D6.5. The report provides a model advancement as well to take into account heat transfer through the

walls of a storage tank and discharge pipe, along with the engineering tool description for modelling transient release during a tank blowdown.

References

Bell I.H., Wronski J., Quoilin S. and Lemort V. (2014), *Pure and Pseudo-pure Fluid Thermophysical Property Evaluation and the Open-Source Thermophysical Property Library CoolProp*, Industrial & Engineering Chemistry Research, Vol. 53 No. 6, 2498–2508.

Cirrone, D., Makarov, D. and Molkov, V. (2019), *Cryogenic hydrogen jets: flammable envelope size and hazard distances for jet fire*, International Conference on Hydrogen Safety, Adelaide, Australia.

Molkov, V., Makarov, V. and Bragin, M. V. (2009), *Physics and modelling of under expanded jets and hydrogen dispersion in atmosphere*, Physics of Extreme States of Matter, pp. 146–149.

A2.2 DISCHA tool, for physical properties and discharge calculations (NCSRD)

DISCHA tool can be applied to calculate accurate physical properties of pure substances and perform discharge calculations either in transient (blowdown) or in steady-state mode with account of discharge line.

A model to estimate steady state two-phase choked flows release rate without account of discharge line effects is available in (Venetsanos and Giannissi, 2017) and (Venetsanos, 2018).

An advanced version of the tool allows accounting for discharge line friction and extra resistances and is able to predict the choked / expanded mass flow rate and distribution of all relevant physical quantities along the discharge line. Single-phase physical properties and vapour-liquid equilibrium are modelled using the Helmholtz Free Energy formulation of (Leachman *et al.*, 2009). Physical properties within the two-phase regime are modelled using the Homogeneous Equilibrium Mixture (HEM) model as in (Venetsanos, 2018).

Calculation procedure is described in (Venetsanos, 2019) and (Venetsanos *et al*., 2021).

References

Leachman, J.W., Jacobsen, R. T., Penoncello, S.G., and Lemmon, E.W. (2009), *Fundamental Equations of State for Parahydrogen, Normal Hydrogen, and Orthohydrogen*, J. Phys. Chem. Ref. Data, 38, 721-748.

Venetsanos, A.G., and Giannissi, S.G. (2017), *Release and dispersion modeling of cryogenic under-expanded hydrogen jets*, Int. J of Hydrogen Energy, 42 (11), 7672-7682.

Venetsanos, A.G. (2018), *Homogeneous non-equilibrium two-phase choked flow modelling*, Int. J. of Hydrogen Energy, 43 (50), 22715-22726.

Venetsanos, A.G. (2019), *Choked two-phase flow with account of discharge line effects*, ICHS-8, Adelaide, Australia, 26-28 Sept. 2019

Venetsanos, A.G., Giannissi, S., Tolias, I., Friedrich, A., Kuznetsov, M. (2021, a) Cryogenic and ambient gaseous hydrogen blowdown with discharge line effects, 9th Int. Conf. on Hydrogen Safety, 21-23 Sept. 2021, Edinburgh, UK.

Venetsanos A.G., Ustolin F., Tolias I., Giannissi S., Momferatos G., Coldrick S., Atkinson G., Lyons K., Jallais S. (2021, b), *Discharge modelling of HSE-LH_2 experiments*, 9th Int. Conf. on Hydrogen Safety, 21-23 Sept. 2021, Edinburgh, UK.

A2.3 The similarity law for concentration decay in momentum jets (UU)

The similarity law for expanded and under-expanded jets allows calculating the axial hydrogen concentration decay in cryogenic momentum-controlled jets. Most jet releases from a cryo-compressed hydrogen storage are expected to be momentum-controlled. The similarity law provides a conservative estimation in case a jet is buoyancy-controlled, as this is expected to have a faster decay (Molkov, 2012). The tool is available on the e-laboratory platform developed within Net-Tools (https://elab-prod.iket.kit.edu/).

A practical application of the similarity law is to estimate the distance from the nozzle where a concentration of interest is reached, e.g. the Lower Flammability Limit (LFL). The similarity law by (Chen and Rodi, 1980) is formulated as:

$$C_{ax} = 5.4 \sqrt{\frac{\rho_N}{\rho_s}} \frac{d}{x}$$

where ρ_N is the density of hydrogen at the nozzle, ρ_s is the density of the surrounding air, d is the nozzle diameter and x is the distance from the release point. Parameters at the real nozzle may be calculated by the under-expanded jet theory developed at Ulster (Molkov *et al.*, 2009).

The similarity law for concentration decay in momentum-dominated expanded jets was validated against releases with temperature 80 K and pressure in the range 2.6-400 bar (Saffers and Molkov, 2013). For a temperature as low as 50 K, the similarity law was validated against release pressure in the range 2-5 bar (Cirrone *et al.*, 2019).

Example

Let us consider a release from a hydrogen storage with temperature 80 K and pressure 200 bar. Nozzle diameter is 1.25 mm. Ambient conditions are temperature of 288 K and pressure of 1 bar. Calculated density at the orifice is 25.08 kg/m^3. The similarity law is applied to calculate the distance where the LFL is reached, to assess the size of the flammable envelope. Distance corresponding to LFL results is 10.6 m.

References

Chen, C. and Rodi, W. (1980), *Vertical Turbulent Buoyant Jets - a review of experimental data*, Pergamon Press, Oxford.

Cirrone D., Makarov D., Molkov, V. (2019), *Cryogenic hydrogen jets: calculation of hazard distances*. International Conference on Hydrogen Safety, 24th-26th September 2019, Adelaide, Australia.

Molkov, V., Makarov, V. and Bragin, M. V. (2009), *Physics and modelling of underexpanded jets and hydrogen dispersion in atmosphere*, Physics of Extreme States of Matter, pp. 146–149.

Molkov, V. (2012), *Fundamentals of Hydrogen Safety Engineering I*, Free-download electronic book available at www.bookboon.com, 2012.Download free books at bookboon.com.

Saffers, J. B. and Molkov, V. V. (2013), *Towards Hydrogen Safety Engineering for Reacting and non-Reacting Hydrogen Releases,* Journal of Loss Prevention in the Process Industries, vol. 26, no. 2, pp. 344–350.

A2.4 Evaluation of LH_2 pools spreading rate (INERIS)

HyPond is a single algebraic formula estimating the maximum extent of a liquid pool likely to spread on the ground following a low-pressure spillage of liquid hydrogen. Maximum extent refers to a free expansion of the pool over a flat, free of obstacles and horizontal surface.

The maximum radius of the pool is obtained by equating the mass flowrate of vaporized hydrogen to that of the LH_2 feeding mass flow rate, and by considering only thermal conduction through the ground as the unique source of heat under a quiet boiling regime:

$$r_{pond} = \sqrt{\frac{Q_m \cdot L_{vap} \cdot \sqrt{\pi \cdot a_{diff}}}{k \cdot \pi \cdot (T_{ground} - T_{eb})}} \cdot t^{\frac{1}{4}}$$

where Q_m is the LH_2 mass flow rate, Q_{cond} the thermal exchange between the pool and the ground, L_{vap} the heat of vaporization of LH_2, k the thermal conductivity of the ground, a_{diff} the thermal diffusivity of the ground and t the time elapsed since the start of the release. A_{pond} is the area of the pool and is linked to the characteristic radius r_{pond} of the pond as: $A_{pond} = \pi \cdot r_{pond}^2$.

The models are established under the assumption of a flat, free of obstacles, non-porous and horizontal surface. Estimation can be valid only for long duration spills (longer than 10-20 s), for which a quiet boiling mode can be assumed. The present model should not be used for catastrophic failures leading to very short duration of the spills, as very different boiling regimes may verify leading to much larger heat fluxes through the ground (one order of magnitude difference).

Example

Let us consider a 0.42 kg/s LH_2 spill with duration of 60 s. The ground substrate is made of aluminium, which has a density of 2750 kg/m^3, specific heat of 900 J/kgK, thermal conductivity of 220 J/mK and thermal diffusivity of $8.85.10^{-5}$ m^2/s. The calculated radius of the pool is 0.37 m.

Appendix 3. Engineering tools for ignition of cold hydrogen mixtures

Appendix 3 presents the engineering correlations and tools supporting the guidelines related to ignition of cryogenic releases that were developed and validated within PRESLHY project. Each section describes briefly the aim of the tool, the implementation procedure, the validation range and an example of application. The full description, including how the engineering correlations and tools were obtained and the validation process, is reported in detail in PRESLHY deliverable D6.5 "Detailed description of novel engineering correlations and tools for LH_2 safety, version 2".

A3.1 Assessment of ignition energy for hydrogen air mixtures (UU)

The present analytical model is aimed at determining the Minimum Ignition Energy (MIE) in hydrogen-air mixtures with arbitrary concentration and initial temperature. The model uses the laminar flame thickness to determine the critical flame kernel. The calculation requires several steps:

1. Estimate the thermo-physical properties for the unburnt (*u*) and burnt (*b*) mixture of given H_2 concentration in air and temperature by using Figure A3.1 or Figure A3.2.

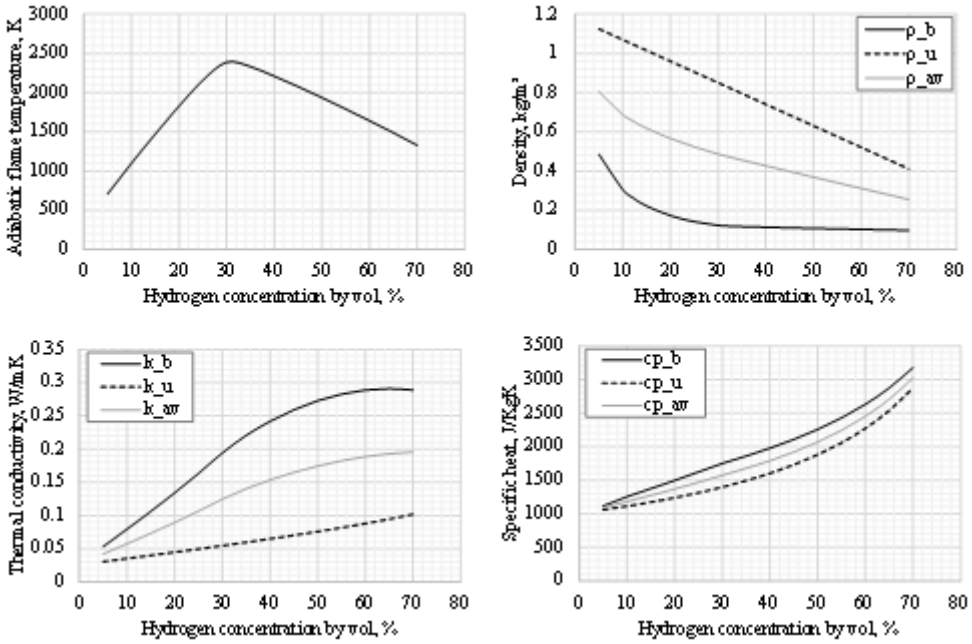

Figure A3.1: Thermo-physical properties of the unburnt and burnt mixture as function of hydrogen concentration in air for ambient temperature (T_u=298K).

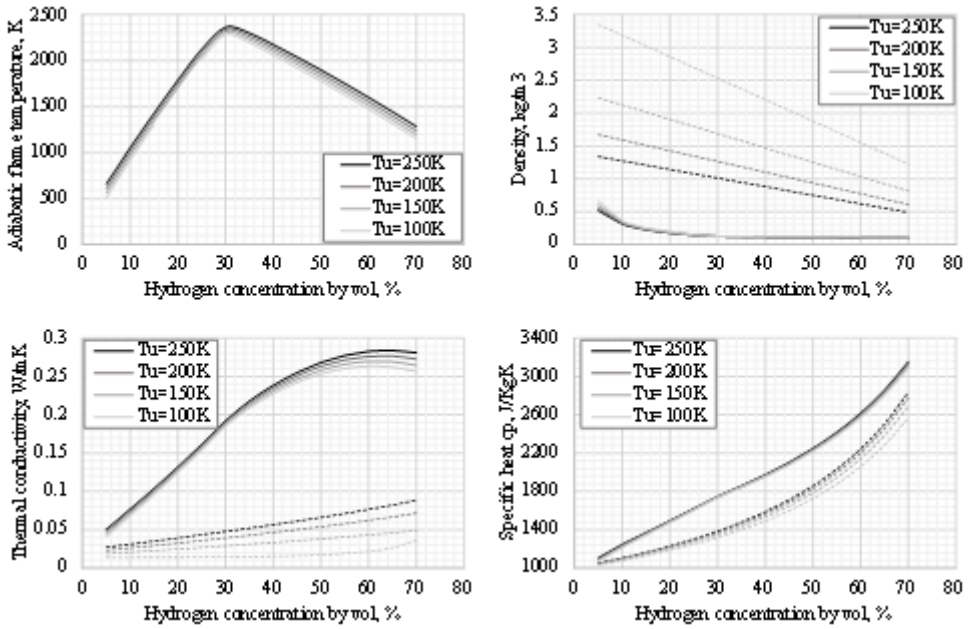

Figure A3.2: Thermo-physical properties of the unburnt (dashed lines) and burnt mixture (solid lines) as function of hydrogen concentration in air for temperature T_u=100-250 K.

2. Estimate the unstretched laminar flame speed, S_u^0, as in Figure A3.3.

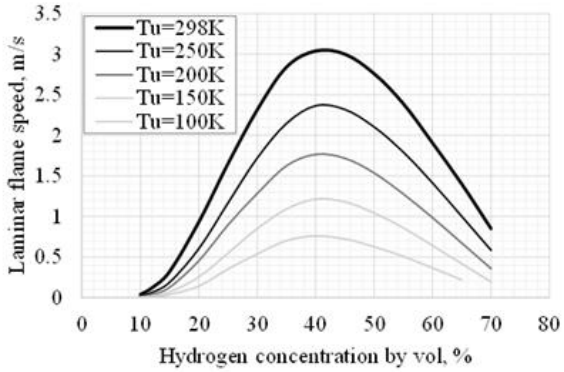

Figure A3.3: Unstretched laminar flame speed calculated through Chemkin software as a function of hydrogen concentration in air and temperature of the unburnt mixture.

3. Correct the unstretched laminar flame speed to include effect of both flame stretch and selective diffusion:

$$S_u^{SD} = X_{SD} S_u^0$$

The corrective factor X_{SD} can be calculated as follows:

$$X_{SD} = 12980 \cdot (C_{H_2})^{-2.98} \text{ for } C_{H_2} < 20\%$$

$$X_{SD} = 100 \cdot (C_{H_2})^{-1.2} \text{ for } 20\% \leq C_{H_2} < 35\%$$

$$X_{SD} = 1 \text{ for } C_{H_2} \geq 35\%$$

where C_{H_2} is the percentage of hydrogen concentration in air.

4. Estimate the laminar flame thickness by Blint's correlation reported in (Poinsot and Veynante, 2005):

$$\delta_L^B = 2\delta \frac{\frac{k_b}{c_{p,b}}}{\frac{k_u}{c_{p,u}}}$$

where δ is the so-called "diffusive" flame thickness, defined by the authors as:

$$\delta = \frac{k_u}{\rho_u c_{p,u} S_u^{SD}}$$

with k_u is the thermal conductivity, ρ_u is the density and $c_{p,u}$ is the specific heat at constant pressure for the unburnt mixture.

5. Estimate the critical flame kernel diameter as $d = 2.5\delta_L^B$.
6. Calculate the MIE as the amount of energy required to heat up a sphere of flammable mixture with diameter of the critical flame kernel at initial temperature T_u of the unburnt mixture, to that of the flame, T_b (Lewis and Elbe, 1961):

$$E_{min} = \frac{1}{6}\pi d^3 \rho_{av} C_{p,av} (T_b - T_u)$$

The model has been validated for mixtures with hydrogen concentration in air within range 9-70% and initial temperature in range 173-300K. The model may be applied to mixtures with initial temperature down to 80 K with hydrogen concentration within range 10-65%.

Example

Let us consider a mixture with H_2=30% by vol. in air and temperature 173 K. The resulting ignition energy is 66 μJ.

References

Lewis, B. and Elbe, G. von. (1961), *Combustion, Flames and Explosions of Gases*, Zeitschrift Für Physikalische Chemie, Vol. 36, Academic Press, New York, available at:https://doi.org/10.1524/zpch.1963.36.3_4.136.

Poinsot, T. and Veynante, D. (2005), *Theoretical and Numerical Combustion*, Second Edition, Decision Support Systems, Second., R.T. Edwards, Inc., P.O., Philadelphia, PA, USA, available at: https://doi.org/10.1016/j.dss.2003.08.004.

A3.2 Assessment of electrostatic charge generated in cold hydrogen releases (PS)

The present engineering tool, abbreviated as ElFiBU, aims at the assessment of electrostatic field built-up during hydrogen releases through a nozzle with circular aperture.

The results of PRESLHY experimental campaign were used to derive a set of empirical correlations to assess the electrostatic field built-up during hydrogen releases through a nozzle with circular aperture, as shown in Figure 4. Only experimental results for reservoir temperatures of approximately 80 K were used, since the experiments at ambient temperature did not generate relevant electric fields.

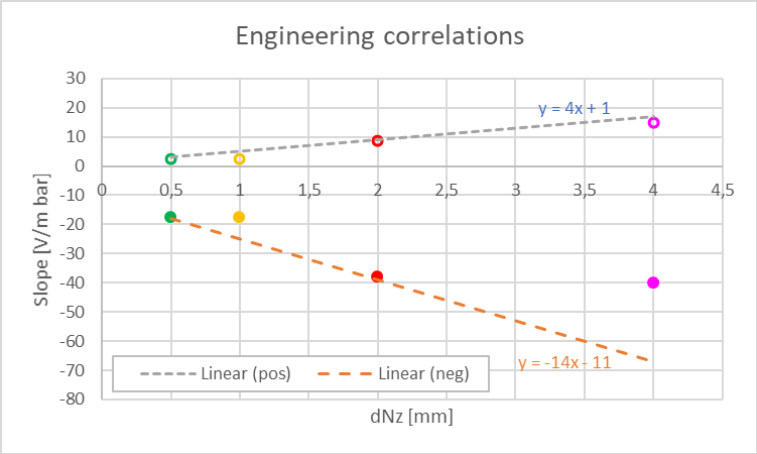

Figure A3.4: Derivation of the factors for the engineering correlations for the estimation of field built-up.

The correlations estimate the generation of both positive field and negative fields for a given nozzle diameter, dNz in mm, and initial pressure, p_{ini} in bar:

Positive Field Built-up: $E(+) \leq (4 \cdot dNz + 1) \cdot p_{ini}$

Negative Field Built-up: $E(-) \leq (-14 \cdot dNz - 11) \cdot p_{ini}$

(The formulas might be used as a kind of rule of thumb and so the units do not match. Corresponding units can be added to slope and intercept of the linear equation in brackets)

The correlations were validated for hydrogen releases at a temperature of 80 K, initial pressure within range 5-200 bar, release diameter from 0.5 to 4 mm.

Example

Let us assume a hydrogen release with temperature and pressure equal to 80 K and 200 bar respectively. Nozzle diameter is 2 mm. The maximum positive electric field is calculated as 900 V/m, whereas the minimum negative electric field is -3900 V/m.

Appendix 4. Engineering tools for liquid and cryogenic hydrogen fires

Appendix 4 presents the engineering correlations and tools supporting the guidelines related to liquid and cryogenic hydrogen fires that were developed and validated within PRESLHY project. Each section describes briefly the aim of the tool, the implementation procedure, the validation range and an example of application. The full description, including how the engineering correlations and tools were obtained and the validation process, is reported in detail in PRESLHY deliverable D6.5 "Detailed description of novel engineering correlations and tools for LH2 safety, version 2".

A4.1 Determination of flame length (UU)

The dimensionless correlation for hydrogen jet flames by Molkov and Saffers (2013) calculates the flame length knowing the storage conditions. The tool is available on the e-laboratory platform developed within Net-Tools (https://elab-prod.iket.kit.edu/). Figure A4.1 shows the dimensionless hydrogen flame length correlation against the experimental data employed for a validation of the tool in Molkov and Saffers (2013) and in Cirrone *et al.* (2019). Dimensionless variable X is defined as follows:

$$X = \frac{\rho_N}{\rho_s} \cdot \left(\frac{u_N}{C_N}\right)^3$$

where ρ_N is the density of hydrogen at the nozzle, ρ_s is the density of the surrounding air, u_N is the velocity at the nozzle, C_N is the speed of sound corresponding to conditions at the nozzle. Parameters at the nozzle exit can be calculated through the under-expanded jet theory developed at Ulster (Molkov *et al.*, 2009) and validated as well against the cryogenic releases included in the validation range of the flame correlation (Cirrone *et al.*, 2019).

Once X is calculated, Figure A4.1 allows to retrieve the ratio $\frac{L_f}{d}$, where L_f is the flame and d the release diameter.

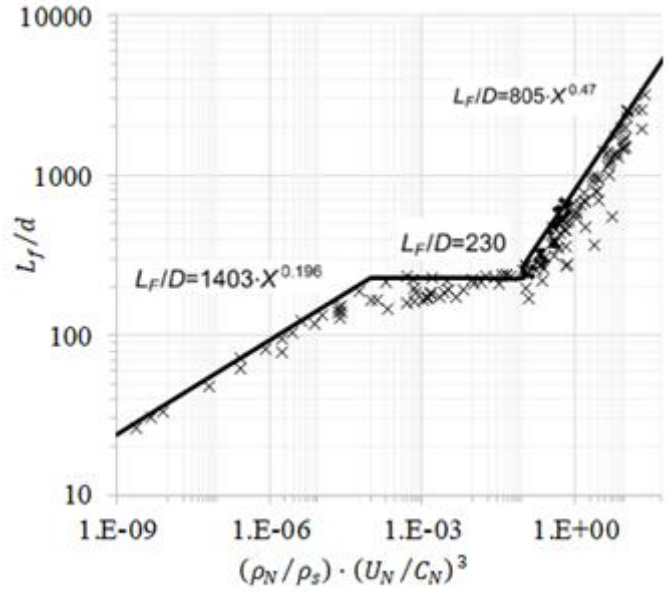

Figure A4.1: The dimensionless correlation for hydrogen jet flames: "+" data from Molkov and Saffers (2013); "♦" data from Cirrone et al. (2019).

The correlation is valid for laminar and turbulent flames, buoyancy - and momentum-controlled fires, expanded (subsonic and sonic) and under-expanded (sonic and supersonic) jet fires.

The dimensionless correlation for hydrogen jet flames was validated against jet fires with pressure in the range 10-900 bar and temperature in the range 187-300 K in (Molkov and Saffers, 2013), and against experiments with release temperature down to 46 K for pressure in the range 2-6 bar abs in (Cirrone *et al*., 2019).

Example

Let us consider a release from a hydrogen storage with temperature 80 K and pressure 200 bar. Nozzle diameter is 2 mm. Ambient conditions are temperature of 288 K and pressure of 1 bar. Calculated density at the orifice, ρ_N, is 25.08 kg/m^3 while velocity, u_N, is 736 m/s. The resulting flame length is 6.65 m.

References

Cirrone, D., Makarov, D., Molkov, V. (2019), *Cryogenic Hydrogen Jets: Calculation of Hazard Distances*. International Conference on Hydrogen Safety, 24th-26th September 2019, Adelaide, Australia.

Molkov, V., Makarov, V. and Bragin, M. V. (2009), *Physics and modelling of underexpanded jets and hydrogen dispersion in atmosphere*, Physics of Extreme States of Matter, pp. 146–149.

Molkov, V. (2012), *Fundamentals of Hydrogen Safety Engineering I*, Free-download electronic book available at www.bookboon.com, 2012. Download free books at bookboon.com.

Molkov, V. and Saffers, J. B. (2013), *Hydrogen Jet Flames*, International Journal of Hydrogen Energy, vol. 38, no. 19, pp. 8141–8158.

A4.2 Determination of thermal load from cryogenic jet fires (UU)

The tool proposed in the present section aims at the assessment of the radiative heat flux in the surrounding of hydrogen jet fires from vertical and horizontal releases of hydrogen at ambient and cryogenic temperature. The tool is based on the weighted multi source flame radiation model developed by Hankinson and Lowesmith (2012) and further expanded by Ekoto *et al.* (2014) for application to large-scale flames. Within the framework of PRESLHY project, UU adapted the model to include evaluation of flame length and width through the dimensionless correlation presented earlier on, and expand the validation range to cryogenic hydrogen jet fires.

The radiative heat flux reaching the target depends on the total surface emissive power of the flame, *S*, the location of the target with respect of the flame, expressed through the view factor *VF*, and the amount of radiation absorbed in the path from the flame to the target, expressed by the atmospheric transmissivity τ:

$$q = \frac{VF}{A_f} \cdot S \cdot \tau$$

Assessment of the radiative heat flux is not a trivial task and calculation requires several steps, assuming known storage pressure and temperature, and release nozzle:

1. Estimate the hydrogen release mass flow rate $\dot{m}$, through the under-expanded jet theory in Section A2.1.

2. Estimate the flame length through the dimensionless correlation presented in Section A4.1., whereas the flame width is calculated as $W_f \approx 0.17 \cdot L_f$, see Schefer *et al.* (2006) and Houf *et al.* (2007).

3. Calculate the flame density, ρ_f, through the following expression:

$$\rho_f = \frac{P_{amb} \cdot MW_{st}}{R_u \cdot T_{ad}}$$

where P_{amb} is the ambient pressure, MW_{st} is the stoichiometric molecular weight of the hydrogen combustion products in air (MW_{st}=24.52 g/mol) and R_u is the universal gas constant (R_u =8314.47 g/(kmol·K)).

4. Estimate the flame residence time t_f (ms) as in Turns and Myhr (1991):

$$t_f = \frac{\pi}{12} \frac{\rho_f \cdot W_f^2 \cdot L_f \cdot Y_s}{\dot{m}}$$

where Y_s is the hydrogen stoichiometric mass fraction (Y_s =0.0281) and ρ_f is the flame density.

5. Evaluate the radiant fraction χ, i.e. the ratio of the energy effectively emitted by the flame as radiation and the chemical energy associated to the fuel stream, as in Molina *et al.* (2007):

$$\chi = 0.08916 \cdot log_{10}\left(t_f \cdot \alpha_f \cdot T_{ad}^4\right) - 1.2172$$

where α_f is the Plank's mean absorption coefficient for water vapour, assumed to be equal to 0.23 m^{-1} based on a study by Ekoto *et al.* (2014), and T_{ad} is the adiabatic flame temperature, which is assumed to be 2390 K for hydrogen combustion in air.

6. Estimate the surface emissive power *S*:

$S = \chi \cdot \dot{m} \cdot \Delta H_c$

where ΔH_c is the gas heat of combustion ($\Delta H_{c,H20} = -119\ MJ/kg$).

7. Use the weighted multi source model by Hankinson and Lowesmith (2012) to decompose the jet flame axis in N radiation emitting points, with N decided accordingly to the characteristics of the problem.

$$\tau \frac{VF}{A_f} = \sum_{i=1}^{N} \frac{w_i \cdot cos\ cos\ \varphi_i}{4 \cdot \pi \cdot r_i^2} \cdot \tau_i$$

where r_i is the distance between the observer and the point source, φ_i is the angle between the observer unit normal and the i-emitter, w_i is the emitter strength parameter and τ_i is the atmospheric transmissivity related to the point source i. Each point along the flame has a different contribution on the final balance of the heat flux, depending on its position along the jet flame axis. It is assumed a linear increase of contribution if the emitting point is located between the point of release and $0.6L_f$, individuated by the point n=0.6N and a linear decrease if the point is located in the remaining part of the jet flame axis:

The air transmissivity is estimated by the empirical correlation (Wayne, 1991):

$$\tau = 1.006 - 0.01171\ [X(H_2O)\ ] - 0.02368\ [X(H_2O)\ ]^2 - 0.03188\ [X(CO_2)\ ] + 0.001164\ [X(CO_2)\ ]^2$$

where L is the path length (m), R_H is the fractional relative humidity, S_{mm} is the saturated vapour pressure of water at atmospheric temperature T (mmHg).

8. Estimate the total radiative heat flux at the receiver as:

$$q = \sum_{i=1}^{N} \frac{w_i \cdot cos\ cos\ \beta_i}{4 \cdot \pi \cdot D_i^2} \cdot \tau_i \cdot S$$

9. Calculate the thermal dose as a function of the exposure duration (*t*, s) in addition to the incident radiative heat flux (*I*, kW/m^2):

$$TD = \int_0^t I(t)^{4/3} dt$$

.

The thermal dose (TD) is expressed in terms of [(kW/m^2)$^{4/3}$s].

The model was validated against hydrogen jet fires with pressure in the range 2-900 bars and temperature in the range 48-315 K.

Example

Let us consider a hydrogen jet fire released from a storage at pressure 3 bar, temperature of 75 K and nozzle diameter (d) of 1.25 mm. Hydrogen is stored at ambient temperature. The release is vertical and originates at the location (0, 0, 0). The location of the receiver is (x_t, y_t, z_t)=(0.2,0.48,0). The receiver is exposed to the flame for 20 s. Ambient temperature and pressure are 288 K and 101325 Pa.

The resulting flame length is 0.73 m long. The received radiative heat flux is 3.43 kW/m^2, whereas the cumulated thermal dose in 20s is 103.46 [(kW/m^2)$^{4/3}$s].

References

Ekoto, I.W., Ruggles, A.J., Creits, L.W., Li, J.X. (2014), *Updated jet flame radiation modelling with buoyancy corrections*, International Journal of Hydrogen Energy 39, 20570-20577.

Hankinson, G. and Lowesmith, B.J. (2012) *A consideration of methods of determining the radiative characteristics of jet fires*. Combustion and Flame, 159 (3), 1165 - 1177.

Houf, W. and Schefer, R. (2007) *Predicting radiative heat fluxes and flammability envelopes from unintended releases of hydrogen*, International Journal of Hydrogen Energy 32, 136-151.

Molina, A., Schefer, R.W. and Houf, W.G. (2007) *Radiative fraction and optical thickness in large-scale hydrogen-jet fires*, Proceedings of the Combustion Institute 31, 2565-2572.

Schefer, R.W., Houf, W.G., Bourne, B., Colton, J. (2006) e*Spatial and radiative properties of an open-flame hydrogen plume*, International Journal of Hydrogen Energy 31, 1332-1340.

Turns, S.R. and Myhr, F.H. (1991) *Oxides of nitrogen emissions from turbulent jet flames: Part I -Fuel Effects and Flame Radiation*, Combustion and Flame 87, 319–335.

Wayne, F. D. (1991) *An economical formula for calculating atmospheric infrared transmissivities*, Journal of Loss Prevention in the Process Industries 4, Issue 2, 86-92.

A4.3 Determination of pressure load from delayed ignition of turbulent jets (UU)

The semi-empirical correlation presented here aims at predicting the maximum overpressure generated by delayed ignition of a hydrogen jet at an arbitrary location for known storage pressure and release diameter. The similitude analysis has been applied to build a correlation. The dimensionless overpressure generated by delayed ignition of hydrogen jets at an arbitrary location, $\frac{\Delta P_{exp}}{P_0}$, is correlated to the dimensionless parameter composed of the product of the ratio of the dimensionless storage pressure, $\sqrt{\frac{P_s}{P_0}}$, and the square of ratio of release diameter to the distance between the centre of the fast burning

mixture in the jet (25-35% by volume) and the target location, $\left(\frac{d}{R_w}\right)^2$. The semi-empirical correlation can be used to estimate the pressure at the target location as follows:

$$\Delta P_t = P_0 \cdot 5000 \cdot \left[\left(\frac{P_s}{P_0}\right)^{0.5} \cdot \left(\frac{d}{R_w}\right)^2 \cdot X_T\right]^{0.95}$$

where $X_T = 1$ is a corrective factor depending on the temperature of the release and the associated expansion coefficients' ratio. This is $X_T = 1$ for ambient temperature releases, whereas for releases at cryogenic temperature is defined as follows:

$$X_T = \frac{T_S}{T_0}\frac{E_{I,T_S}}{E_{I,T_0}}$$

A best-fit correlation has been withdrawn as follows:

$$\Delta P_t = P_0 \cdot 92.4 \cdot \left[\left(\frac{P_s}{P_0}\right)^{0.5} \cdot \left(\frac{d}{R_w}\right)^2 \cdot X_T\right]^{0.76}$$

The semi-empirical correlation was built using approximately 80 experiments from literature and PRELSHY project, seventeen of which were performed at cryogenic temperature (80 K). The correlation is applicable for hydrogen storage pressure 0.5-65 MPa and release diameter 0.5-52.5 mm.

Example

Let us consider a hydrogen tank having a storage pressure of 35 MPa (P_s) and nozzle diameter (d) of 2 mm. Hydrogen is stored at ambient temperature. The release is horizontal and originates at the location (0, 1, 0). The location of the receiver is (x_t, y_t, z_t) = (2, 1, 2). Ambient temperature and pressure are 288 K and 101325 Pa.

1. The similarity law (see Appendix 2, Section A2.3) is used to calculate the location in the jet with hydrogen concentration equal to 30%, which corresponds to the centre of the fast burning hydrogen-air cloud:

$$x_{30\%} = 5.4\sqrt{\frac{\rho_N}{\rho_S}}D\frac{C_N}{C_{30\%}} = 1.3\ m$$

2. The distance between the fast burning cloud and the target location can be calculated as follows by knowing the respective coordinates:

$$R_w = \sqrt{(x_{30\%} - x_t)^2 + (y_{30\%} - y_t)^2 + (z_{30\%} - z_t)^2} = 2.1\ m$$

3. The pressure at the target location can conservatively be calculated as:

$$\Delta P_t = P_0 \cdot 5000 \cdot \left[\left(\frac{P_s}{P_0}\right)^{0.5} \cdot \left(\frac{d}{R_w}\right)^2 \cdot X_T\right]^{0.95} = 14.53\ kPa$$

The developed correlation may be used inversely to estimate the hazard distances corresponding to defined harm criteria for people. In this example, a "no harm" overpressure of 1.35 kPa is considered, according to the harm criteria proposed in (Baker

et al., 1983). A "injury" and "fatality" limit were considered to be 16.5 kPa and 100 kPa respectively, following the harm criteria proposed in (Mannan, 2005):

$$R_{no\_harm} = 7.4\ m;$$

$$R_{Injury} = 2.0\ m;$$

$$R_{Fatality} = 0.8\ m$$

The maximum hazard distance from the release source will be reached along the jet axis and can be calculated as:

$$x_{no\_harm} = x_{30\%} + R_w = 8.7\ m$$

The distances from the release source for the "injury" and "fatality" limit can be calculated similarly as 3.3 and 2.1 m respectively.

References

Baker, W.E., Cox, P.A., Kulesz, J.J. Strehlow, R.A. and Westine, P.S. (1983), Explosion Hazards and Evaluation, Elsevier

Mannan, S. (2005), Lee's Loss Prevention in the Process Industries.

A4.4 Determination of laminar burning velocity and expansion ratio for hydrogen air mixtures (INERIS)

Graphical information and correlations are established to estimate the influence of the temperature on the laminar burning velocity of the flame and of the expansion ratio of the combustion for hydrogen air mixtures as function of fuel air ratios. The pressure is atmospheric. The ranges of variations are intended to represent those potentially occurring during a leakage of liquid hydrogen. Results were obtained from the experimental campaigns performed by INERIS within PRESLHY project (Proust, 2021). The graphical values and correlations are valid in the temperature range -100°C to ambient and at atmospheric pressure.

The evolution of the measured laminar burning velocity as a function of the temperature and of the mixture composition can be retrieved from Figure A4.2.

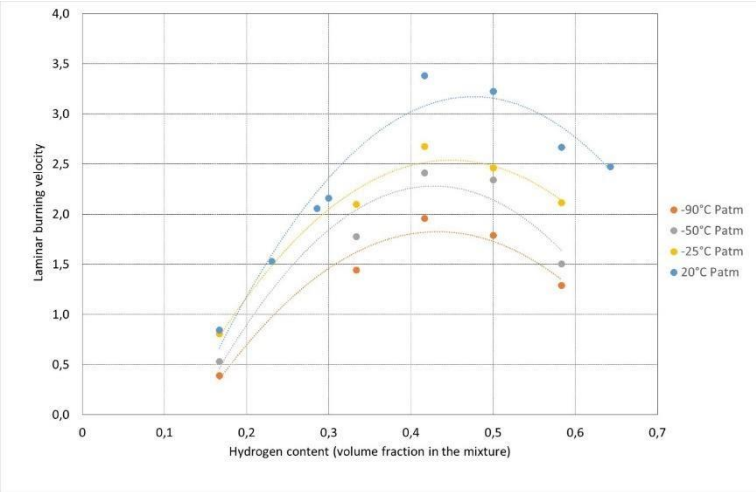

Figure A4.2: Evolution of the laminar burning velocity as function of the temperature and of the mixture composition.

The maximum laminar burning velocity correlates correctly with the following power law in the temperature range -100°C to +250°C:

$$\frac{Slmax_T}{Slmax_{Tref}} = \left(\frac{T}{T_{ref}}\right)^{1.48}$$

where S_{lmaxT} is the maximum laminar burning velocity at temperature T (in K) and $S_{lmaxTref}$ is the maximum laminar burning velocity at the reference temperature T_{ref} (in K). Atmospheric pressure is considered.

The expansion ratio, i.e. the ratio between the volumes of the mixture before the combustion and after, can be retrieved from Figure A4.3. Data were obtained from a thermodynamic equilibrium code used at CEA (Gordon and McBride, 1994).

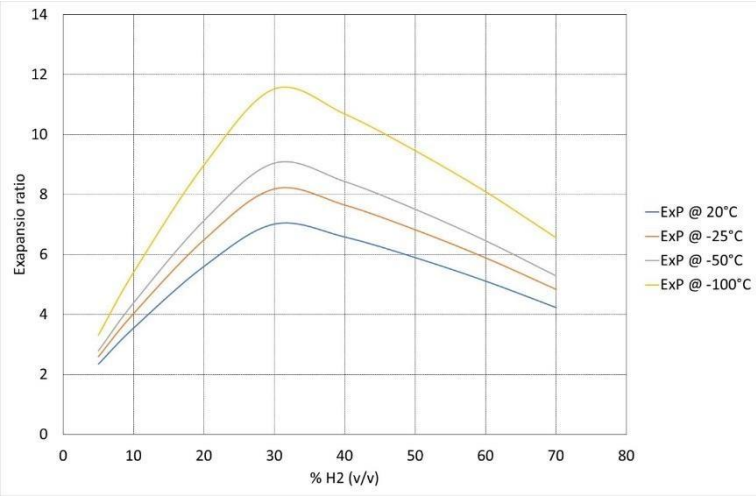

Figure A4.3: Evolution of the expansion ratio of the combustion as function of the temperature and of the mixture composition.

The theory of the adiabatic combustion tells that the expansion ratio should vary proportionally to the inverse of the absolute temperature:

$$\frac{Exp_T}{Exp_{Tref}} = \frac{T_{ref}}{T}$$

where Exp_T is the expansion ratio at temperature T (in K) and Exp_{Tref} is the expansion ratio at the reference temperature T_{ref} (in K). Atmospheric pressure is considered. Proportionality is approximately true.

References

Gordon S., McBride B. J. (1994), *Computer program for calculation of complex chemical equilibrium compositions and applications, Part 1: Analysis*, NASA reference publication 1311.

Proust C. (2021), *Summary of experiment series E4.1 results (Ignition parameters), Deliverable D21*, EU Project Pre-normative REsearch for Safe use of Liquid Hydrogen (PRESLHY), FCH 2 JU, Grant Agreement N. 779613.

A4.6 Fireball size after liquid hydrogen spill combustion (UU, KIT)

The present correlation determines a fireball size after liquid hydrogen spill combustion by Makarov *et al.* (2021). The correlation was built based on the best fit of experimental data in Zabetakis (1964):

$$D_{bf} = 8.16m^{0.45}$$

A second correlation provides a conservative correlation to estimate a fireball size from combustion of LH_2 spills:

$$D_c = 10m^{0.45}$$

Example

Let us consider a spill of 0.2 kg of LH_2. The conservative fireball size after the LH_2 spill combustion can be calculated as 4.85 m.

References

Makarov, D., Shentsov, V., Kuznetsov, M. and Molkov, V. (2021) *Hydrogen Tank Rupture in Fire in the Open Atmosphere: Hazard Distance Defined by Fireball*, Hydrogen, Vol. 2 No. 1, pp. 134–146.

Zabetakis, M.G. *Flammability Characteristics of Combustible Gases and Vapors*; Bureau of Mines: Pittsburgh, PA, USA, 1964.

Appendix 5. Engineering tools for deflagration and DDT in cold H_2 air mixtures

Appendix 5 presents the engineering correlations and tools supporting the guidelines related to deflagration and DDT in cold H_2-air mixtures that were developed and validated within PRESLHY project. Each section describes briefly the aim of the tool, the implementation procedure, the validation range and an example of application. The full description, including how the engineering correlations and tools were obtained and the validation process, is reported in detail in PRESLHY deliverable D6.5 "Detailed description of novel engineering correlations and tools for LH_2 safety, version 2".

A5.1 Flame acceleration and detonation transition for cryogenic hydrogen air mixtures (KIT, PS)

The present model allows evaluating critical hydrogen concentrations and conditions for effective flame acceleration (FA) and Detonation-to-Deflagration Transition (DDT) at cryogenic temperatures of the hydrogen-air mixtures. Such conditions depend on the geometry of the system mixture characterisation, history and dynamics of the combustion process. Full description is available in (PRESLHY D6.5).

Within the flammability limits, three typical combustion regimes can be distinguished for gaseous mixtures:

- slow subsonic deflagrations ($v < c_r$ - flame velocity v is less than the speed of sound in reactants c_r),
- fast supersonic flame ($c_r < v < c_p$ - flame velocity is less than the sound speed in products c_p, but more than the sound speed in reactants)
- detonation ($v = D_{CJ}$, Chapman-Jouguet velocity).

All possible regimes and characteristic pressure profiles based on paper (Dorofeev *et al.*, 2001) are shown in Figure A5.1 for hydrogen-air mixtures at initial pressure of 1 bar.

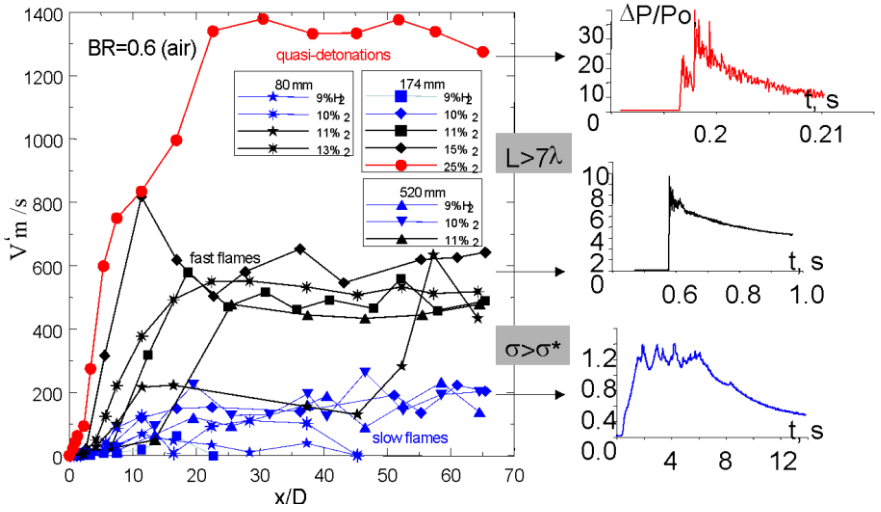

Figure A5.1 Combustion regimes for hydrogen-air mixtures in a tube geometry (Dorofeev et al., 2000; 2001).

Mixtures with the expansion rate σ, i.e. the ratio of densities of unburned material ρ_u to the density of combustion products ρ_b, above the critical value σ* can effectively accelerate to the speed of sound and then detonate, if the detonation criteria $L > 7\lambda$ is satisfied (L is the characteristic size of the combustible domain; λ is the detonation cell size). The mixtures with $\sigma < \sigma^*$ cannot accelerate to the speed of sound and only subsonic combustion regimes may occur.

The determination of flame acceleration and Detonation-to-Deflagration Transition for a given hydrogen concentration in air, system geometry and blockage ratio (BC) requires several steps, which are summarised as follows.

1. Determine the Blockage Ratio BR

Blockage ratio is the ratio of blocked area to the channel cross section area. For cylinder tube geometry, it can be expressed as follows:

$$BR = 1 - \frac{d^2}{D^2}$$

where *d* is the orifice diameter of the open area; D is the inner tube diameter. For complex geometry, the blockage ratio can be expressed as follows:

$$BR = \sum A_i / A$$

where A_i is the total area of each visible object blocking the channel cross-section *A*.

2. Determine conditions for flame acceleration

For hydrogen-air mixtures at ambient conditions, the critical expansion ratio is σ* = 3.75 (Dorofeev *et al.*, 2001). It corresponds to 11% of hydrogen in the mixture.

Experimental data of PRESLHY project (Kuznetsov *et al.*, 2021) and Dorofeev *et al.*, 2001) were used to approximate the dependence of the limit conditions between slow (M<1) and fast sonic deflagration (M>1) on initial temperature T [K] for the range T = 90-650K as follows (see Figure A5.2):

$$\sigma^* = 2200 * T^{-1.12}$$

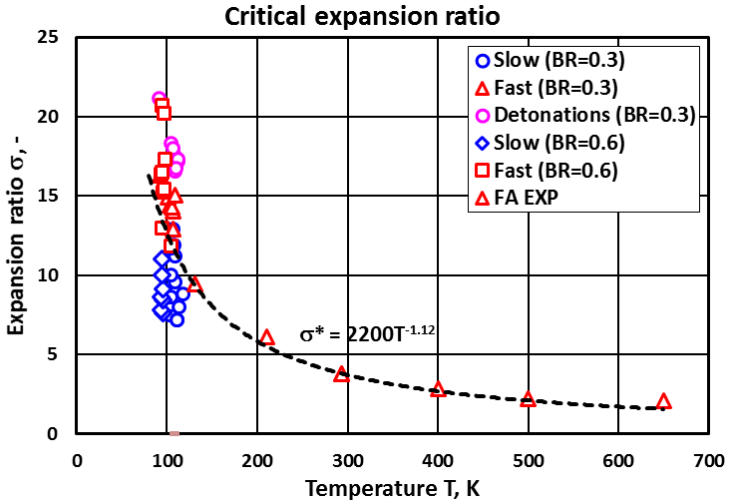

Figure A5.2: Critical expansion ratio as function of initial temperature based on experiments in obstructed tubes (BR=0.3 and BR=0.6): black dashed line is the border between slow and fast flames.

Experimentally, it was found the critical expansion ratio σ* = 12.5 at 100 K of initial temperature of the gas. In terms of hydrogen concentration, it corresponds to about 16% H_2 in air.

Figure A5.3 shows the dependence of hydrogen concentrations $[H2]_{cr}$ corresponding to critical expansion ratio σ* as a function of initial temperature. The dependence can be approximated as a polynomial function of initial temperature and might be more useful for practical application than the critical expansion ratio:

$$[H_2]cr = 4.817 * 10^{-5}T^2 - 0.0441T + 19.96$$

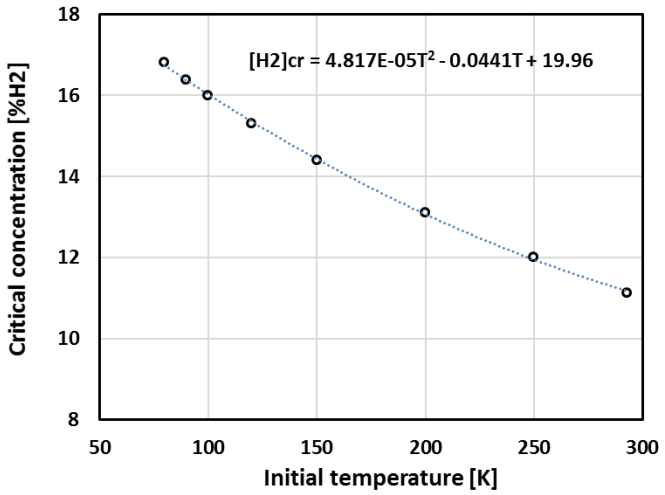

Figure A5.3 Hydrogen concentrations corresponding to critical expansion ratio as a function of initial temperature as expressed here before.

3. Determine the detonation cell size

The detonation cell size λ is the measure of detonability to be used to evaluate the detonation propagation and detonation transition criteria:

$D = \lambda/\pi$ smooth tube (BR = 0-0.1)

$d = \lambda$ obstructed tube (BR = 0.3)

$d = 3\lambda$ obstructed tube (BR = 0.6)

$d = 10\lambda$ obstructed tube (BR = 0.9)

The data at cryogenic temperature T = 100K experimentally obtained for cryogenic temperature (T=100K) in (Kuznetsov *et al.*, 2021) and at ambient temperature (T=293K) calculated by CELL_H2 code (Gavrikov *et al.*, 2000), are used to approximate the detonation cell sizes as polynomial dependence on hydrogen concentration in volumetric percent $[H_2]$:

$$\lambda = 0.0006724[H_2]^4 - 0.1039[H_2]^3 + 6.0786[H_2]^2 - 159.74[H_2] + 1603.3$$

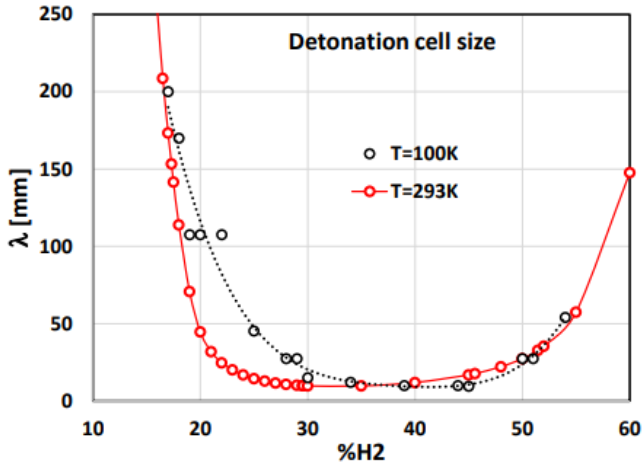

Figure A5.4: Experimental detonation cell size at cryogenic temperature T=100K in comparison with the data at ambient temperature T = 293K.

4. Determine the run-up distance to detonation

The run-up-distance to detonation depends on mixture reactivity (expressed in terms of laminar flame speed and detonation cell size) and level of turbulence. Both factors can promote flame acceleration and shorten the run-up distance X_D.

The run-up distance to detonation at cryogenic temperatures was experimentally found to be two times shorter than at ambient conditions:

$X_D = 500\lambda$ smooth tube (BR = 0)

Experimental data in (Kuznetsov *et al.*, 2002) can be used to estimate the run-up distances as function of blockage ratio:

X_D = (10-12)D (BR = 0.3)

X_D = (3-4)D (BR = 0.6)

X_D = (2-3)D (BR = 0.9)

5. Determine the pre-detonation length, L

Characteristic size *L* for detonation onset is formulated depending on the size of the channel *D*, dimension of unobstructed passage between obstacle and sidewall *d* and spacing between repeating obstacles *S*:

$$L = \frac{D + S}{2\left(1 - d/D\right)}$$

For an equidistant spacing between vehicles *S* = *D*, a function of blockage ratio BR and an equivalent diameter D can be used:

$$L = \frac{D}{1-\sqrt{1-BR}}$$

6. Determine Detonation onset. DDT conditions

The model includes the DDT criterion as dimensionless ratio L/λ of the characteristic size *L* over the detonation cell size λ as a measure of detonability of the mixture:

$$L/\lambda > N^*$$

where *N** is the critical value for detonation onset (DDT) or detonation propagation dependent on the geometry of the system. The values of critical factor N* are collected in Table 1 for several most useful geometries of the channel. We suppose that the DDT criterion does not change at cryogenic conditions. The only change that could occur is the detonation cell size.

Table 1. Dimensionless scale for different processes.

Dimensionless scale	**Critical value N*, (-)**	**Detonation relevant phenomenon**	**References**
D/λ	$1/\pi$	Detonation propagation in a smooth channel with diameter *D*	Moen *et al.* (1981)
d/λ	1	Detonation propagation in obstructed tubes with orifice size *d* (BR*<0.43)	Teodorczyk *et al.* (1988)
d/λ	3	Detonation propagation in obstructed tubes with orifice size *d* (BR*=0.6)	Teodorczyk *et al.* (1988), Kuznetsov *et al.* (2000)
d/λ	10	Detonation propagation in obstructed tubes with orifice size *d* (BR*=0.9)	Veser *et al.* (2002)
L/λ	7	Detonation onset in obstructed channels (0.1<BR*<0.6)	Dorofeev *et al.* (2000)

Table 2 summarizes the results for the critical ratios for DDT as a function of blockage ratio by using equations at calculation step 2.

Table 2. Critical ratios for DDT as function of blockage ratio.

Blockage ratio BR	*L/D*	*D/λ*	*d/λ*
0.1	19.49	0.36	0.34
0.2	9.47	0.74	0.66
0.3	6.12	1.14	0.96
0.4	4.44	1.58	1.22
0.5	3.41	2.05	1.45
0.6	2.72	2.57	1.63

Both of aforementioned criteria for flame acceleration and DDT also require the satisfaction of so-called run-up distance (RUD) criterion $X_D < L$, where L is the characteristic length of the channel (Veser et al., 2002; Kuznetsov et al., 2005;, Ciccarelli et al., 2008). X_D is the distance required for flame acceleration and detonation preconditioning. If dimension L is longer than the run-up-distance to the speed of sound X_D then the detonation may occur.

7. Estimate the strength of explosion

Maximum combustion pressure is the integral characteristic of the combustion process, which depends on energy of combustion and dynamics of flame propagation. Theoretically, the maximum combustion pressure for sonic deflagration is of the order adiabatic combustion pressure *Picc*. For detonation, the characteristic pressure is the Chapman-Jouguet pressure, P_{CJ}. The STANJAN code (Reynolds, 1986) and Cantera code (Goodwin, 2001) based on NASA thermodynamic databases were used to calculate the *Picc* pressure and Chapman-Jouguet pressure, see Figure A5.5 and Figure A5.6 for a graphical estimation.

Alternatively, the maximum combustion pressures at cryogenic temperature P(T) can be calculated from the reference data at ambient conditions $P(T_0)$ times the temperature factor (Table 3):

$$P_{icc}(T) = P_{icc}(T_0)\left(\frac{T_0}{T}\right)$$

$$P_{CJ}(T) = P_{CJ}(T_0)\left(\frac{T_0}{T}\right)$$

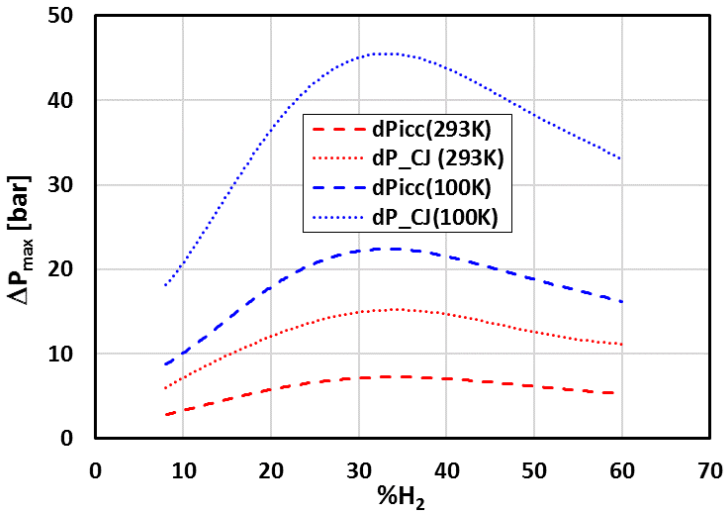

Figure A5.5: Maximum combustion pressure for different hydrogen-air mixtures at cryogenic temperature T=100K in comparison with the data at ambient temperature T = 293K.

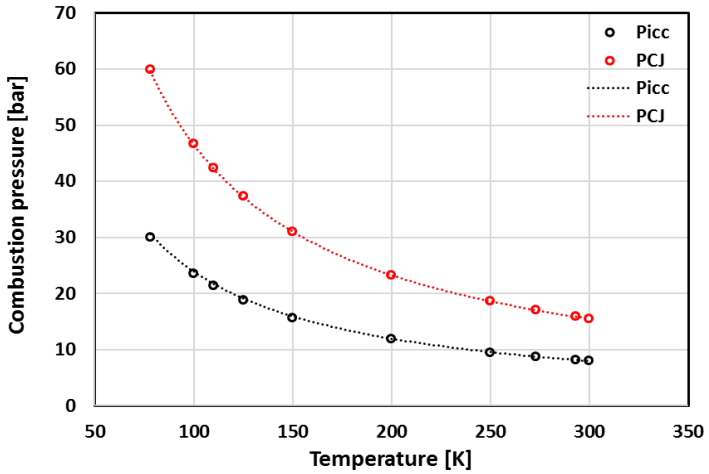

Figure A5.6: Chapman-Jouguet detonation pressure P_{CJ} and adiabatic combustion pressure P_{icc} as a function of initial temperature for stoichiometric hydrogen-air mixture: open points – calculations by STANJAN code; dashed lines – calculation by equations.

Table 3. Main properties of hydrogen-air combustible mixtures at T=293K.

H_2 mole fraction* X_{H2}	Picc [bar]	P_CJ [bar]	H_2 mole fraction X_{H2}	Picc [bar]	P_CJ [bar]
0.08	3.80	7.12	0.25	7.74	15.06
0.09	4.10	7.72	0.296	8.26	16.10
0.1	4.39	8.31	0.3	8.29	16.14
0.11	4.67	8.87	0.35	8.27	16.13
0.12	4.94	9.42	0.4	8.00	15.60
0.13	5.20	9.95	0.45	7.66	14.91
0.14	5.46	10.47	0.5	7.28	14.14
0.15	5.71	10.97	0.55	6.85	13.27
0.16	5.95	11.46	0.6	6.38	12.32
0.18	6.41	12.38	0.65	5.87	11.30

0.2	6.84	13.24	0.7	5.32	10.20
0.22	7.23	14.03	0.75	4.73	9.01

* The data for intermediate concentration can be linearly or by spline interpolated.

During the combustion process, the flame can accelerate to the speed of sound or to detonation. Thus, characteristic combustion pressure should be of the order of P_{icc} or P_{CJ}. In case of transient regime, a gas dynamic dependence can be used in an assumption that flow velocity behind shock wave is equal to visible flame velocity:

$$\frac{P_2}{P_1} = \frac{2\gamma}{\gamma+1} M^2 - \frac{\gamma-1}{\gamma+1}$$

where P_2 is the dynamic combustion pressure in our case; P_1 is the initial pressure 1 bar; γ is the adiabatic coefficient of burned composition; M = v/c is the Mach number as a ratio of flow (fame) velocity v = Uf over the speed of sound in reactants c = cr. Figure A5.7 shows the dynamic pressure at cryogenic temperature T = 100K and ambient temperature comparison for a stoichiometric hydrogen-air mixture.

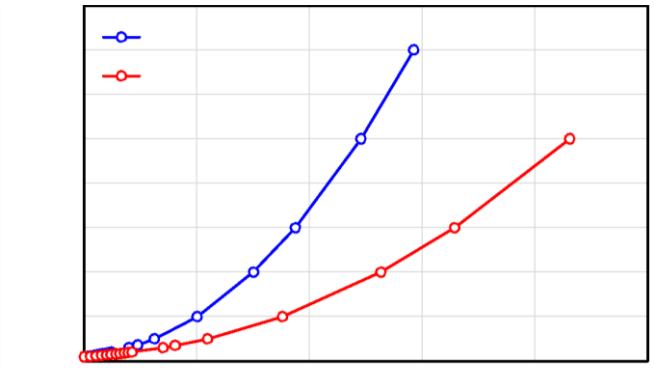

Figure A5.7: Dynamic pressure as a function of flow velocity calculated for stoichiometric hydrogen air at two temperatures.

Table 4. Main properties of hydrogen-air combustible mixtures at T=100K.

H2 mole fraction* X_{H2}	Expansion ratio** σ [-]	Sound speed in reactants cr [m/s]	Sound speed in products cp [m/s]	Adiabatic combustion pressure Picc [bar]	Detonation pressure P_CJ [bar]
0.08	7.30	208	554	8.44	18.46
0.09	8.03	209	582	9.34	20.27
0.1	8.73	210	608	10.21	22.02
0.11	9.42	211	633	11.06	23.72
0.11	9.42	211	633	11.06	23.72
0.12	10.10	212	657	11.88	25.36
0.15	12.04	216	723	14.21	30.03
0.16	12.66	218	744	14.94	31.51
0.17	13.27	219	764	15.65	32.93
0.18	13.87	220	784	16.34	34.31

0.19	14.45	222	803	17.01	35.65
0.2	15.02	223	821	17.66	36.95
0.22	16.13	226	857	18.89	39.43
0.25	17.67	231	906	20.57	42.82
0.28	19.02	235	946	21.99	45.70
0.29	19.38	237	956	22.34	46.37
0.3	19.59	239	966	22.56	46.82
0.34	19.18	246	997	22.39	46.55
0.39	18.25	256	1014	21.47	44.65
0.44	17.22	266	1029	20.37	42.42
0.45	17.01	269	1032	20.14	41.95
0.5	15.90	281	1046	18.91	39.46
0.51	15.67	284	1048	18.65	38.94
0.54	14.97	292	1056	17.85	37.34
0.58	13.99	305	1066	16.73	35.08
0.6	13.49	312	1070	16.15	33.91

* The data for intermediate concentration can be linearly or by spline interpolated.

** Main properties calculated by STANJAN, Cantera and NIST Standard Reference Database (Goodwin, 2001; Reynolds, 1986; Manion et al., 2015).

*** Detonation cell sizes calculated with CELL_H2 program based on (Gavrikov et al., 2000).

The model can be used at atmospheric pressure of 1 bar within the temperature range from 90K to 293K and hydrogen concentrations from 8 to 60 vol. %. The model covers elongated structures as tubes, channels, sequences of rooms with smooth and rough walls. It also considers the blockage of channels from 10 to 60%.

References

Ciccarelli, G., Dorofeev, S. (2008) *Flame acceleration and transition to detonation in ducts*, Progress in Energy and Combustion Science, Volume 34, Issue 4, 499-550.

Dorofeev S.B., Sidorov V. P., Kuznetsov M. S., Matsukov I. D., Alekseev V. I. (2000), *Effect of scale on the onset of detonations*. Shock Waves, v. 10, 137-149.

Dorofeev S.B., Kuznetsov M.S., Alekseev V.I., Efimenko A.A., Breitung W. (2001), *Evaluation of limits for effective flame acceleration in hydrogen mixtures*. Journal of Loss Prevention in the Process Industries, Vol 14/6, 583-589.

Gavrikov, A.I., Efimenko, A.A., Dorofeev, S.B. (2000), *A model for detonation cell size prediction from chemical kinetics*, Combustion and Flame, Vol. 120, Issues 1–2, 19-33.

Goodwin, D.G. (2001), Cantera User's Guide, Cal. Institute of Techn., Pasadena, CA.

Kuznetsov M.S., Alekseev V. I., Dorofeev S. B. (2000), *Comparison of critical conditions for DDT in regular and irregular cellular detonation system*s. Shock Waves 10, 217-224.

Kuznetsov, M., Alekseev, V., Matsukov, I. (2002), *Deflagration-to-Detonation Transition in H_2 -Air and H_2 -O_2 -N_2 mixtures in channels with obstructions*. Advances in Confined Detonations, Torus Press Ltd., Moscow, 26-30.

Kuznetsov M., Alekseev V., Matsukov I., Dorofeev S. (2005), *DDT in a Smooth Tube filled with Hydrogen-Oxygen Mixtures*. Shock Waves, vol. 14, No 3, 205-215.

Kuznetsov, M., Denkevits, A., Veser, A., Friedrich, A., Necker, G., Jordan, T. (2021) *Shock tube experiments on flame propagation regimes and critical conditions for flame acceleration and detonation transition for hydrogen-air mixtures at cryogenic temperatures*. Submitted to ICHS9, Edinburgh, UK, 2021.

Manion, J.A., Huie, R.E., Levin, R.D., Burgess Jr., D.R., Orkin, V.L., Tsang, W., McGivern, W.S., Hudgens, J.W., Knyazev, V.D., Atkinson, D.B., Chai, E., Tereza, A.M., Lin, C.-Y., Allison, T.C., Mallard, W.G., Westley, F., Herron, J.T., Hampson, R.F. Frizzell, D.H. (2015), NIST Chemical Kinetics Database, NIST Standard Reference Database 17, Version 7.0 (Web Version), Release 1.6.8, Data version 2015.09, National Institute of Standards and Technology, Gaithersburg, Maryland, 20899-8320. Web address: http://kinetics.nist.gov/

Moen, I. O., Donato, M., Knystautas, R., Lee, J. H. S. (1981), *The influence of confinement on the propagation of detonations near the detonability limit*. Symp. (Int.) Combust., 18th, pp. 1615--23. Pittsburgh, Pa : Combust. Inst.

Reynolds, W.C. (1986), *The Element Potential Method for Chemical Equilibrium Analysis: Implementation in the Interactive Program STANJAN Version 3*, Dept. of Mechanical Engineering, Stanford University, Palo Alto, California, January 1986.

Teodorczyk, A., Lee, J.H., Knystautas, R. (1988), *Propagation mechanism of quasi-detonations.* 22nd Symposium (Int.) on Combustion. The Combustion Institute, Pittsburgh,1723–173.

Veser, A., Breitung, W., Dorofeev, S.B. (2002), *Run-up distances to supersonic flames in obstacle-laden tubes*, J. Phys. IV France, 12, No 7, 333-340.